Chapter 7
Handling of Race Cars

Race cars come in a number of shapes, sizes, engine power, type of wings, etc. However, most of them share the following features relevant to handling:

1. four wheels (two axles);
2. two-wheel drive;
3. *aerodynamic devices* (and hence, significant aerodynamic downforces, along with significant aerodynamic drag);
4. *limited-slip or locked differential*;
5. often no intervention by electronic active safety systems like ABS or ESP.

The handling analysis of race cars is more involved than that of road cars (Chap. 6). The non-open differential makes the vehicle behavior very sensitive to the *turning radius*, while the aerodynamic effects make the vehicle handling behavior very sensitive to the *forward speed*.

7.1 Assumptions for Race Car Handling

The analysis developed here is based on the vehicle model introduced in Chap. 3 and summarized in Sect. 3.15. However, it is recommended to read also Chaps. 5 and 6 as a primer for vehicle handling.

For definiteness, let us suppose to deal with a *rear-wheel-drive* vehicle. Owing to the presence of a *limited-slip differential* and of relevant *aerodynamic loads* (high downforce and hence high drag), the tires of the driven axle undergo significant longitudinal slips under almost all operating conditions. Therefore, it does not make much sense to restrict the analysis to steady state since the very beginning.

The original version of this chapter was revised: Belated corrections have been incorporated. The correction to this chapter is available at https://doi.org/10.1007/978-3-319-73220-6_12

M. Guiggiani, *The Science of Vehicle Dynamics*,
https://doi.org/10.1007/978-3-319-73220-6_7

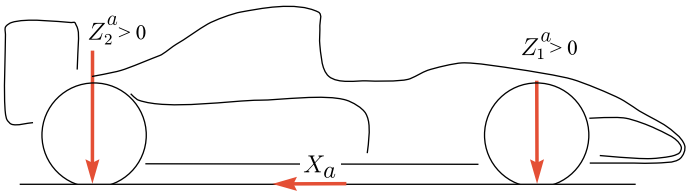

Fig. 7.1 Aerodynamic drag and downforces (all positive)

To highlight the role of the limited-slip differential, we do not consider the vehicle while braking,[1] but only during power-on/power-off conditions. Therefore, we have at the front axle negligible longitudinal tire forces, that is

$$F_{x_{11}} = F_{x_{12}} = 0 \quad \text{and hence} \quad \sigma_{x_{11}} = \sigma_{x_{12}} = 0 \tag{7.1}$$

7.1.1 Aerodynamic Downloads

Many race cars have wings and underbody diffuser to create, at high speed, downforces that press the race car against the surface of the track. Therefore, the vertical loads acting on the tires can be very speed dependent.

Aerodynamic forces have been discussed in Sect. 3.7.2. The overall aerodynamic load can be correctly and conveniently represented as in Fig. 7.1. At high speed, Z_1^a and Z_2^a, and also the aerodynamic drag X_a, have fairly high positive values.

7.1.2 Limited-Slip Differential

Race cars are usually equipped with a *limited-slip differential*, that is a differential with a torque bias, which can become totally locked[2] in some cases.

Torque bias means that the torques applied to the left and right shafts may not be equal to each other. Therefore, as shown in Fig. 7.2, we may have

$$F_{x_{21}} \neq F_{x_{22}} \tag{7.2}$$

In a curve, counterintuitive as it may appear, the inside wheel has not necessarily an angular speed lower than the outside wheel. Just consider a race car accelerating

[1] Braking of formula cars is discussed in Sect. 4.11.

[2] A *locked differential* is actually not a differential. Indeed, a differential mechanism must convey power from a single shaft to two shafts while permitting different rotation speeds. A locked differential no longer has this degree of freedom and the *two wheels must rotate at the same angular speed*.

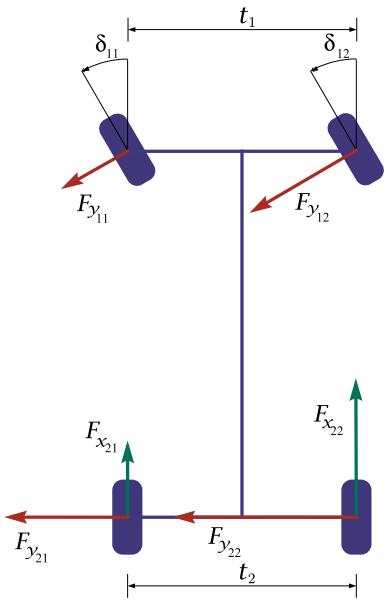

Fig. 7.2 Road-tire grip forces for a car with limited-slip differential (cf. Fig. 6.1)

while exiting a curve: in some cases, due to the still high lateral acceleration, its inside wheel is barely touching the ground, and hence it is probably spinning faster than the outer wheel (Fig. 3.55c). This phenomenon is one of the main reasons that makes a limited-slip differential almost mandatory in a race car. Otherwise, that is with an open differential, the car would not accelerate much, as the maximum longitudinal force would be limited by the inner wheel (the one barely touching the ground). On the other hand, if a vehicle is turning at low lateral acceleration, the inside wheel will be turning slower than the outside wheel, and hence it will receive more torque (Fig. 3.55a).

To make the torques applied to the left and right shafts not equal to each other, limited-slip differentials are built to have some sort of *friction* inside the housing. Indeed, a limited-slip differential is characterized by its internal efficiency $\eta_h \ll 1$, and hence by a Torque Bias Ratio (TBR $= 1/\eta_h$) $\gg 1$. The mechanics of any differential mechanism has been discussed in Sect. 3.14, where the relevant equations have been obtained.

7.2 Vehicle Model for Race Car Handling

The equations, collected in Sect. 3.15 for the fairly general vehicle model described in Chap. 3, are now tailored to the case of race cars (limited slip differential, non constant forward speed, and aerodynamic downforces).

As in any dynamical system, there are input (known) functions and output (to be found) functions.

Perhaps, the most natural way to set up the problem is to assign as input functions the angular speed $\omega_h(t)$ of the housing of the differential mechanism (Sect. 3.14) and the angular position $\delta_v(t)$ of the steering wheel. Imposing $\omega_h(t)$ is more realistic than imposing directly the forward velocity $u(t)$ (cf. Chap. 6).

The vehicle motion is the sought output. According to Chap. 3, to monitor the vehicle motion we can use, for instance, the forward velocity $u(t)$, the lateral velocity $v(t)$ and the yaw rate $r(t)$.

To link the input to the output we have to build a system of differential-algebraic equations.

7.2.1 Equilibrium Equations

The in-plane equilibrium equations are the most intuitive, and we start with them, with the aid of Figs. 7.1, 7.2 and 7.3.

For a rear-wheel-drive race car, the in-plane equilibrium equations (3.91) become

$$\begin{aligned} ma_x &= X \\ ma_y &= Y \\ J_z\dot{r} &= N \end{aligned} \tag{7.3}$$

or, more explicitly

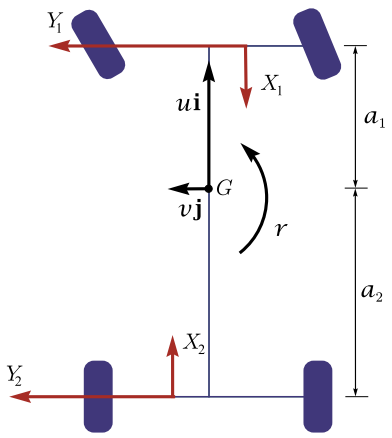

Fig. 7.3 Vehicle model

$$
\begin{aligned}
m(\dot{u} - vr) &= X_1 + X_2 - X_a \\
m(\dot{v} + ur) &= Y_1 + Y_2 \\
J_z\dot{r} &= Y_1 a_1 - Y_2 a_2 + N_X = N_Y + N_X
\end{aligned}
\tag{7.4}
$$

where

$$
\begin{aligned}
X_1 &= -F_{y_{11}} \sin(\delta_{11}) - F_{y_{12}} \sin(\delta_{12}) \\
X_2 &= F_{x_{21}} + F_{x_{22}} \\
X_a &= \frac{1}{2}\rho S C_x u^2 \\
Y_1 &= F_{y_{11}} \cos(\delta_{11}) + F_{y_{12}} \cos(\delta_{12}) \\
Y_2 &= F_{y_{21}} + F_{y_{22}} \\
N_X &= \Delta X_1\, t_1 + \Delta X_2\, t_2
\end{aligned}
\tag{7.5}
$$

with

$$
\begin{aligned}
\Delta X_1 &= \frac{1}{2}\left[F_{y_{11}} \sin(\delta_{11}) - F_{y_{12}} \sin(\delta_{12})\right] \\
\Delta X_2 &= \frac{1}{2}\left(F_{x_{22}} - F_{x_{21}}\right)
\end{aligned}
$$

It is kind of interesting to compare these equations with (6.3).

In any two-axle car, the yawing moment

$$
N_Y = Y_1 a_1 - Y_2 a_2 \tag{7.6}
$$

is always present in the yaw equation, that is in the third equation in (7.4).

The other yawing moment N_X collects two very different contributions.

The contribution $N_f = \Delta X_1 t_1$ comes from the difference between the longitudinal components of the front lateral forces (Fig. 7.4). Therefore, it becomes significant only when the front steer angles are not small, like in FSAE competitions. In other competitions, the front steer angles are usually below 0.2 rad (11°) and hence $\Delta X_1 t_1$ is probably negligible.

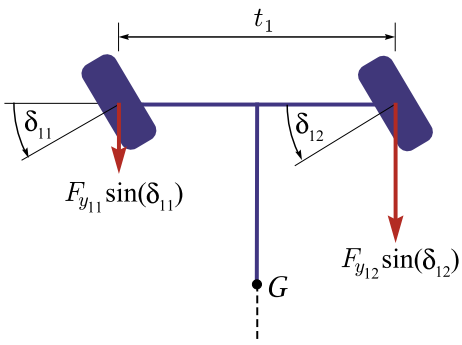

Fig. 7.4 Origin of ΔX_1 (steer angles of about 30°)

The other contribution $N_d = \Delta X_2 t_2$ comes from the limited-slip differential (Fig. 7.2). It involves the difference between the rear tire longitudinal forces. It can be quite relevant, depending on the type of differential and on the operating conditions (lateral acceleration, power-on/power-off, steer angle).

7.2.2 Lateral Forces for Dynamic Equilibrium

Regardless of (7.5), the last two equations in (7.4) can be already solved with respect to the axle lateral forces Y_1 and Y_2, thus getting

$$\begin{aligned} Y_1 &= \frac{1}{l}(ma_2\, a_y + (J_z\dot{r} - N_X)) = Y_1(a_y, \dot{r}, N_X) \\ Y_2 &= \frac{1}{l}(ma_1\, a_y - (J_z\dot{r} - N_X)) = Y_2(a_y, \dot{r}, N_X) \end{aligned} \tag{7.7}$$

A result already obtained in (3.99) and (3.153). The key point is that we can have $(N_Y = J_z\dot{r} - N_X) \neq 0$, even if $\dot{r} = 0$. Therefore, differently from (6.8), Y_1 and Y_2 depend, in general, also on the yawing moment N_X.

7.2.3 Tire Forces

According to the tire constitutive equations (2.85), and taking (7.1) into account, the front tire forces can be expressed as

$$\begin{aligned} F_{x_{11}} &= 0 \\ F_{y_{11}} &= F_{y_{11}}(Z_{11},\ \gamma_{11},\ \sigma_{y_{11}}) \\ F_{x_{12}} &= 0 \\ F_{y_{12}} &= F_{y_{12}}(Z_{12},\ \gamma_{12},\ \sigma_{y_{12}}) \end{aligned} \tag{7.8}$$

where Z_{1j} are the vertical loads, γ_{1j} are the camber angles and $\sigma_{y_{1j}}$ are the lateral theoretical slips.

The rear tires are under combined slip conditions and, therefore, also the longitudinal slips $\sigma_{x_{2j}}$, that is the angular speed of rotation ω_{2j} of each wheel, have to be taken into account

$$\begin{aligned} F_{x_{21}} &= F_{x_{21}}(Z_{21},\ \gamma_{21},\ \sigma_{x_{21}},\ \sigma_{y_{21}}) \\ F_{y_{21}} &= F_{y_{21}}(Z_{21},\ \gamma_{21},\ \sigma_{x_{21}},\ \sigma_{y_{21}}) \\ F_{x_{22}} &= F_{x_{22}}(Z_{22},\ \gamma_{22},\ \sigma_{x_{22}},\ \sigma_{y_{22}}) \\ F_{y_{22}} &= F_{y_{22}}(Z_{22},\ \gamma_{22},\ \sigma_{x_{22}},\ \sigma_{y_{22}}) \end{aligned} \tag{7.9}$$

Here we are assuming that we know the grip available in the contact patch. Of course, this is a rather unrealistic assumption, but we cannot afford in this analysis to model also the phenomenon of grip generation.

We see that these constitutive (tire) equations need additional algebraic equations for the vertical loads Z_{ij}, the camber angles γ_{ij}, the longitudinal and lateral slips $\sigma_{x_{ij}}$ and $\sigma_{y_{ij}}$.

7.2.4 Tire Slips

In general, the rear (driven) tires apply both longitudinal and lateral forces to the vehicle. Therefore, we need all slip components. According to (3.61)

$$\begin{aligned} \sigma_{x_{21}} &= \frac{(u - rt_2/2) - \omega_{21} r_2}{\omega_{21} r_2} \qquad & \sigma_{y_{21}} &= \frac{v - ra_2}{\omega_{21} r_2} \\ \sigma_{x_{22}} &= \frac{(u + rt_2/2) - \omega_{22} r_2}{\omega_{22} r_2} \qquad & \sigma_{y_{22}} &= \frac{v - ra_2}{\omega_{22} r_2} \end{aligned} \tag{7.10}$$

where r_2 is the rolling radius.

In compact form, as in (3.199), we have

$$\begin{aligned} \sigma_{x_{21}} &= \sigma_{x_{21}}(u, r, \omega_{21}) \qquad & \sigma_{y_{21}} &= \sigma_{y_{21}}(v, r, \omega_{21}) \\ \sigma_{x_{22}} &= \sigma_{x_{22}}(u, r, \omega_{22}) \qquad & \sigma_{y_{22}} &= \sigma_{y_{22}}(v, r, \omega_{22}) \end{aligned} \tag{7.11}$$

where

$$\omega_{21} = \omega_h - \Delta\hat{\omega} \qquad \text{and} \qquad \omega_{22} = \omega_h + \Delta\hat{\omega} \tag{7.12}$$

Of course, $\Delta\hat{\omega}(t)$ is unknown (in the sense that it is not an input quantity).

At the front axle we have longitudinal pure rolling and, accordingly, we can rely on the expressions (6.21)

$$\begin{aligned} \sigma_{y_{11}} &= \frac{(v + ra_1)\cos(\delta_{11}) - (u - rt_1/2)\sin(\delta_{11})}{(u - rt_1/2)\cos(\delta_{11}) + (v + ra_1)\sin(\delta_{11})} \\ \sigma_{y_{12}} &= \frac{(v + ra_1)\cos(\delta_{12}) - (u + rt_1/2)\sin(\delta_{12})}{(u + rt_1/2)\cos(\delta_{12}) + (v + ra_1)\sin(\delta_{12})} \end{aligned} \tag{7.13}$$

In compact form

$$\begin{aligned} \sigma_{x_{11}} &= 0 \qquad & \sigma_{y_{11}} &= \sigma_{y_{11}}(u, v, r, \delta_{11}) \\ \sigma_{x_{12}} &= 0 \qquad & \sigma_{y_{12}} &= \sigma_{y_{12}}(u, v, r, \delta_{12}) \end{aligned} \tag{7.14}$$

The steer angles δ_{ij} need additional algebraic equations.

7.2.5 Camber Angles

Let, $\gamma_{i2}^0 = -\gamma_{i1}^0 = \gamma_i^0$ be the camber angles under static conditions (Fig. 7.5), and let $\Delta\gamma_{i1} = \Delta\gamma_{i2} = \Delta\gamma_i$ be the camber variations due to vehicle roll motion (Fig. 7.6).

Like in (6.17), the camber angles of the two wheels of the same axle are thus given by

$$\gamma_{i1} = -\gamma_i^0 + \Delta\gamma_i \qquad \text{and} \qquad \gamma_{i2} = \gamma_i^0 + \Delta\gamma_i \tag{6.17'}$$

where the camber variation $\Delta\gamma_i$, according to (3.110), depends linearly on the roll angles ϕ_i^p and ϕ_i^s, since the term $\pm z_i^s/c_i$ is usually negligible in race cars (Fig. 7.7)

$$\Delta\gamma_i \simeq -\left(\frac{t_i/2 - c_i}{c_i}\right)\phi_i^s + \phi_i^p = \Delta\gamma_i(\phi_i^s, \phi_i^p) \tag{7.15}$$

Different suspensions with the same no-roll center share only the same value of q_i (Fig. 7.7). Therefore they behave differently.

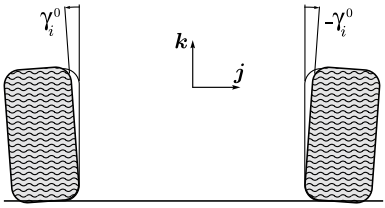

Fig. 7.5 Positive static camber γ_i^0 (front view)

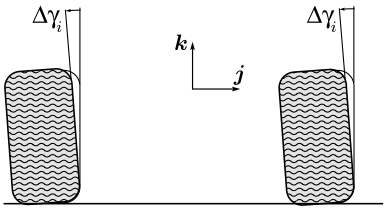

Fig. 7.6 Positive camber variations $\Delta\gamma_i$ due to roll motion (front view)

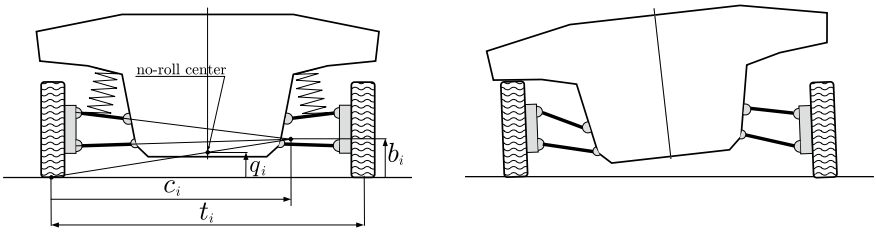

Fig. 7.7 First order suspension parameters for camber variation

Both the roll angles ϕ_i^p, due to the tire deflections, and ϕ_i^s, due to suspension deflections, need additional algebraic equations.

7.2.6 Steer Angles

According to (3.198) we have the following (simplified) expressions for the steering angles of the front wheels

$$\begin{aligned} \delta_{11} &= -\delta_1^0 + \tau_1\delta_v + \varepsilon_1\frac{t_1}{2l}(\tau_1\delta_v)^2 + \Upsilon_1\phi_1^s = \delta_{11}(\delta_v, \phi_1^s) \\ \delta_{12} &= \quad \delta_1^0 + \tau_1\delta_v - \varepsilon_1\frac{t_1}{2l}(\tau_1\delta_v)^2 + \Upsilon_1\phi_1^s = \delta_{12}(\delta_v, \phi_1^s) \end{aligned} \tag{7.16}$$

which are functions of the steering wheel rotation δ_v and of the front suspension roll angle ϕ_1^s.

In (7.16), as discussed in Sect. 3.4, δ_1^0 is the static toe angle, τ_1 is the gear ratio of the whole steering system, ε_1 is the Ackermann coefficient for dynamic toe (Fig. 7.8), and Υ_1 is the roll steer coefficient. Most cars have $\tau_2 = \varepsilon_2 = 0$, that is no direct steering of the rear wheels.

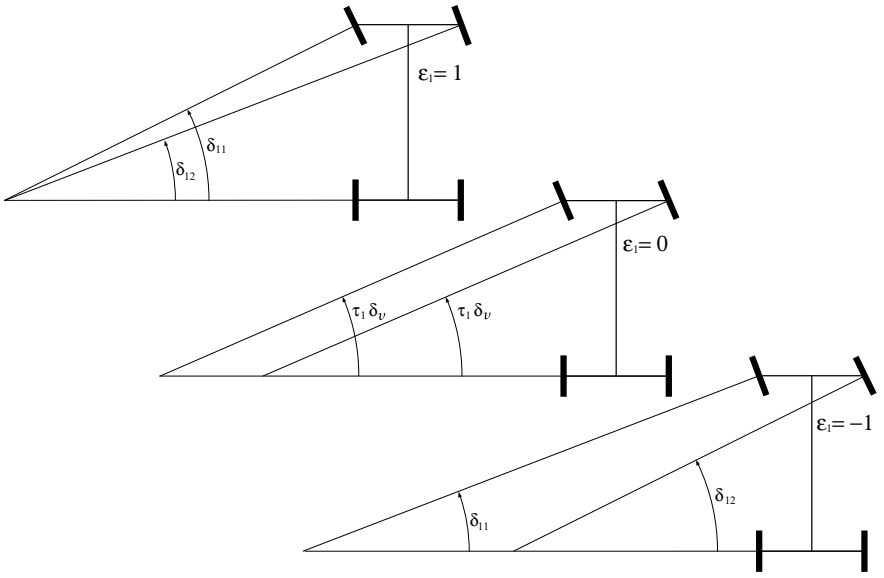

Fig. 7.8 Ackermann steering (top), parallel steering (middle), anti-Ackermann steering (bottom)

Actually, (7.16) is a Taylor series expansion. We believe it is a good way to classify and compare steering geometries. It shows in a quantitative, yet simple, way how much the steering system differs from parallel steering.

7.2.7 *Vertical Loads on Each Wheel*

As shown in (3.105), the vertical load acting on each wheel is the algebraic sum of four contributions (Fig. 7.9):

1. the static load (weight);
2. the aerodynamic load;
3. the longitudinal load transfer;
4. the lateral load transfer.

More explicitly, the expressions (3.106) for the vertical loads on each tire must be taken in full, except for the $J_{zx}r^2$ term, which is almost certainly negligible. In compact form, (3.106) can be recast as (cf. (6.14))

$$\begin{aligned}
Z_{11} &= \frac{1}{2}\left(\frac{mga_2}{l} + \zeta_1 u^2 - \frac{ma_x h}{l}\right) - \Delta Z_1 = Z_{11}(u, a_x, \Delta Z_1)\\
Z_{12} &= \frac{1}{2}\left(\frac{mga_2}{l} + \zeta_1 u^2 - \frac{ma_x h}{l}\right) + \Delta Z_1 = Z_{12}(u, a_x, \Delta Z_1)\\
Z_{21} &= \frac{1}{2}\left(\frac{mga_1}{l} + \zeta_2 u^2 + \frac{ma_x h}{l}\right) - \Delta Z_2 = Z_{21}(u, a_x, \Delta Z_2)\\
Z_{22} &= \frac{1}{2}\left(\frac{mga_1}{l} + \zeta_2 u^2 + \frac{ma_x h}{l}\right) + \Delta Z_2 = Z_{22}(u, ax, \Delta Z_2)
\end{aligned} \tag{7.17}$$

where, according to (3.80) and (4.24)

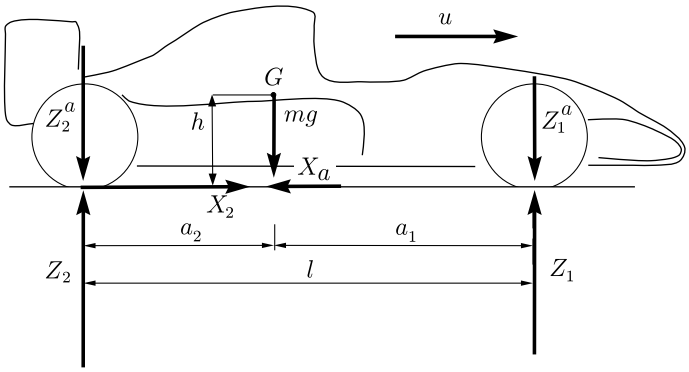

Fig. 7.9 Forces acting on a Formula car

$$\zeta_1 = \frac{1}{2}\rho_a S_a C_{z1} \quad \text{and} \quad \zeta_2 = \frac{1}{2}\rho_a S_a C_{z2} \tag{7.18}$$

A race car with wings has $C_{zi} > 0$, and hence $\zeta_i > 0$ (Fig. 7.1). Of course X_a is always positive (drag).

It is interesting to compare (7.17) with (6.14). There are two important differences:

1. the speed dependent aerodynamic vertical loads;
2. the longitudinal load transfer due to the longitudinal acceleration a_x.

Moreover, there is the effect of the yaw moment N_d on the lateral forces and hence on the lateral load transfers, as discussed hereafter.

7.2.8 *Lateral Load Transfers*

The lateral load transfers ΔZ_i were obtained in (3.148) as linear functions of the axle lateral forces Y_1 and Y_2 (Fig. 7.10)

$$\begin{aligned}
\Delta Z_1 &= \frac{1}{t_1}\left[\frac{k_{\phi_1}}{k_\phi}(Y_1+Y_2)\left(h-q^b\right) + Y_1 q_1 + \frac{k_{\phi_1}k_{\phi_2}}{k_\phi}\left(\frac{Y_2 q_2}{k^p_{\phi_2}} - \frac{Y_1 q_1}{k^p_{\phi_1}}\right)\right] = \Delta Z_1(Y_1, Y_2)\\
\Delta Z_2 &= \frac{1}{t_2}\left[\frac{k_{\phi_2}}{k_\phi}(Y_1+Y_2)\left(h-q^b\right) + Y_2 q_2 + \frac{k_{\phi_1}k_{\phi_2}}{k_\phi}\left(\frac{Y_1 q_1}{k^p_{\phi_1}} - \frac{Y_2 q_2}{k^p_{\phi_2}}\right)\right] = \Delta Z_2(Y_1, Y_2)
\end{aligned} \tag{7.19}$$

where $q^b \simeq q$ (Fig. 7.10).

Synthetically, we have

$$\begin{aligned}
\Delta Z_1 &= \xi_{11} Y_1 + \xi_{12} Y_2\\
\Delta Z_2 &= \xi_{21} Y_1 + \xi_{22} Y_2
\end{aligned} \tag{3.152'}$$

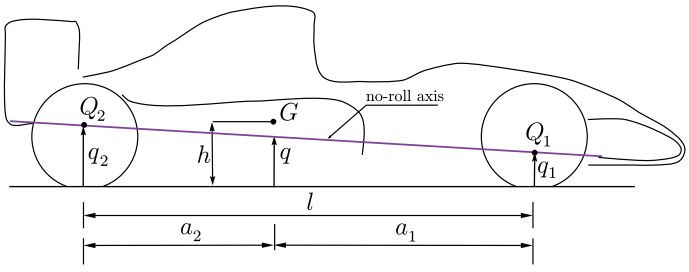

Fig. 7.10 No-roll axis

Owing to (7.7), that is to the moment N_X, mainly due to the limited slip differential, the lateral load transfers no longer depend only on a_y. This is quite a big difference for the complexity of the vehicle dynamic behavior, if compared to (6.9).

7.2.9 Roll Angles

In most race cars the suspension roll stiffnesses $k^s_{\phi_i}$ and the tire roll stiffnesses $k^p_{\phi_1}$ are not very much different. Therefore, assuming rigid tires is not quite correct.

We have the following relationships between the axle lateral forces and the roll angles. According to (3.143), the roll angles (front and rear) due to the tires are

$$\begin{aligned}
\phi_1^p &= \frac{1}{k^p_{\phi_1}} \frac{k_{\phi_1} k_{\phi_2}}{k_\phi} \left[\frac{(Y_1 + Y_2)(h - q^b)}{k_{\phi_2}} + \frac{Y_1 q_1}{k^s_{\phi_1}} + \frac{Y_1 q_1}{k^s_{\phi_2}} + \frac{Y_1 q_1 + Y_2 q_2}{k^p_{\phi_2}} \right] = \phi_1^p(Y_1, Y_2) \\
\phi_2^p &= \frac{1}{k^p_{\phi_2}} \frac{k_{\phi_1} k_{\phi_2}}{k_\phi} \left[\frac{(Y_1 + Y_2)(h - q^b)}{k_{\phi_1}} + \frac{Y_2 q_2}{k^s_{\phi_1}} + \frac{Y_2 q_2}{k^s_{\phi_2}} + \frac{Y_1 q_1 + Y_2 q_2}{k^p_{\phi_1}} \right] = \phi_2^p(Y_1, Y_2)
\end{aligned} \tag{7.20}$$

and, according to (3.144), the roll angles due to the suspension springs are

$$\begin{aligned}
\phi_1^s &= \frac{1}{k^s_{\phi_1}} \frac{k_{\phi_1} k_{\phi_2}}{k_\phi} \left[\frac{(Y_1 + Y_2)(h - q^b)}{k_{\phi_2}} - \frac{Y_1 q_1}{k^p_{\phi_1}} + \frac{Y_2 q_2}{k^p_{\phi_2}} \right] = \phi_1^s(Y_1, Y_2) \\
\phi_2^s &= \frac{1}{k^s_{\phi_2}} \frac{k_{\phi_1} k_{\phi_2}}{k_\phi} \left[\frac{(Y_1 + Y_2)(h - q^b)}{k_{\phi_1}} - \frac{Y_2 q_2}{k^p_{\phi_2}} + \frac{Y_1 q_1}{k^p_{\phi_1}} \right] = \phi_2^s(Y_1, Y_2)
\end{aligned} \tag{7.21}$$

Therefore, in this model, all roll angles are assumed to be linear functions of the axle lateral forces Y_1 and Y_2.

7.2.10 Behavior of the Limited-Slip Differential

In a car equipped with a limited-slip differential the two longitudinal forces $F_{x_{21}}$ and $F_{x_{22}}$, exerted by the rear tires on the vehicle, are not necessarily equal to each other (Fig. 7.2). Therefore we have a *yawing moment* N_d coming from the longitudinal forces acting on the vehicle

$$N_d = \Delta X_2 t_2 = \frac{F_{x_{22}} - F_{x_{21}}}{2} t_2 \tag{7.22}$$

When compared with (6.2), that is with the case of open differential, it looks like a small difference, but it is not. The limited-slip differential does affect quite a bit the vehicle handling behavior, and, accordingly, the vehicle model becomes much

more involved when compared with the model of a vehicle equipped with an open differential.

Another consequence is that we have significant longitudinal forces at the rear wheels and, therefore, significant longitudinal slips, even when turning at constant forward speed

$$F_{x_{2j}} \neq 0 \qquad \text{and hence} \qquad \sigma_{x_{2j}} \neq 0 \tag{7.23}$$

In other words, the longitudinal slips $\sigma_{x_{21}}$ and $\sigma_{x_{22}}$ cannot be neglected, and, hence, the tire constitutive equations (7.9) must include them for the two wheels of the driven axle.

Any differential mechanism provides the same link between the angular velocities of the wheels and the angular velocity ω_h of the housing of the differential

$$\omega_{21} = \omega_l = \omega_h - \Delta\hat{\omega} \qquad \text{and} \qquad \omega_{22} = \omega_r = \omega_h + \Delta\hat{\omega} \tag{7.24}$$

As discussed in Sect. 3.14.9, a limited-slip differential with internal efficiency η_h, provides a link between the longitudinal forces due to the engine power. For a rear driven vehicle we can model it as

$$F_{x_{22}} = \eta_h^{\zeta(t)} F_{x_{21}} \tag{7.25}$$

where

$$\zeta(t) = \frac{\arctan(\chi\, \Delta\hat{\omega}(t))}{\pi/2} \tag{7.26}$$

with χ a positive *big number*, something around 1000 s. This way, the limited-slip differential action is activated whenever $\Delta\hat{\omega}(t)$ has significant values, with a smooth transition through the locked state of the differential ($\Delta\hat{\omega}(t) \simeq 0$). Figures 3.66, 3.67, 3.68, 3.69, 3.70 and 3.71 are applications of this model. By setting $\eta_h = 1$ in (3.184) we obtain the open differential behavior.

7.2.11 Reducing the Number of Equations

To define this vehicle model for race car handling we have introduced three differential equations and quite a bit of algebraic equations. It is possible, and convenient, to reduce the number of algebraic equations by combining them.

From (7.7) we have that the axle lateral forces Y_i are known (linear) functions of the lateral acceleration a_y, of the yaw acceleration $\dot{r}$, and of the moment N_X.

These functions $Y_i(a_y, \dot{r}, N_X)$ can be plugged directly into the expressions of the lateral load transfers $\Delta Z_i(Y_1, Y_2)$, of the suspension roll angles $\phi_i^s(Y_1, Y_2)$ and of the tire roll angles $\phi_i^p(Y_1, Y_2)$.

Then, $\Delta Z_i\big(Y_1(a_y, \dot{r}, N_X), Y_2(a_y, \dot{r}, N_X)\big)$ go into the expressions of $Z_{ij}(u, a_x, \Delta Z_i)$, while the roll angles have to be inserted into the camber angle equations $\gamma_{ij}(\phi_i^s, \phi_i^p)$ and, possibly, into the steer angles $\delta_{ij}(\delta_v, \phi_i^s)$.

The steer angles just obtained have to be plugged into the expressions of the front lateral slips $\sigma_{1j}(v, r, u, \delta_{1j})$.

The rear slips involve the angular velocities of the wheels. It is maybe better to set $\omega_{2j} = \omega_h \pm \Delta\hat{\omega}$, like in (7.24). This way, since ω_h is given, we have that only $\Delta\hat{\omega}$ is unknown.

The just obtained expressions of the vertical loads, of the camber angles, and of the slip components go into the tire constitutive equations (7.8) and (7.9).

Ultimately, all tire force components can be *explicitly*, and easily, set as functions of:

1. the state variables $(u(t), v(t), r(t))$;
2. the accelerations $a_x(t), a_y(t)$ and $\dot{r}(t)$, or, equivalently, the derivatives $(\dot{u}(t), \dot{v}(t), \dot{r}(t))$
3. the angular velocity $\Delta\hat{\omega}(t)$;
4. the moment $N_X(t)$;
5. the given angular velocity $\omega_h(t)$ of the housing of the differential;
6. the given angle $\delta_v(t)$ of the steering wheel.

That is to say that we know all the following algebraic functions

$$\begin{aligned} F_{x_{ij}} &= F_{x_{ij}}\big(u, v, r, a_x, a_y, \dot{r}, \Delta\hat{\omega}, N_X; \omega_h, \delta_v\big) \\ F_{y_{ij}} &= F_{y_{ij}}\big(u, v, r, a_x, a_y, \dot{r}, \Delta\hat{\omega}, N_X; \omega_h, \delta_v\big) \end{aligned} \tag{7.27}$$

It is very important to note that among the arguments of these functions there is the moment N_X, which is defined in (7.5) in terms of some of the tire force components

$$\begin{aligned} N_X &= \Delta X_1\, t_1 + \Delta X_2\, t_2 \\ &= \frac{t_1}{2}\big[F_{y_{11}} \sin(\delta_{11}) - F_{y_{12}} \sin(\delta_{12})\big] + \frac{t_2}{2}\big(F_{x_{22}} - F_{x_{21}}\big) \end{aligned} \tag{7.28}$$

Moreover, the Eq. (7.25) governing the behavior of the limited-slip differential has to be included in the mathematical model

$$F_{x_{22}} = \eta_h^{\left(\frac{\arctan(\chi\,\Delta\hat{\omega})}{\pi/2}\right)} F_{x_{21}} \tag{7.29}$$

The number of algebraic equations has been drastically reduced, but two of them are still there and will be there. Indeed, we have three state variables and three differential equations, but also two other unknown functions ($\Delta\hat{\omega}(t)$ and $N_X(t)$), that require two additional algebraic equations. The two unknown functions "survived" the equation reduction process because, in general, there is no way to "extract" them analytically. Therefore, it is convenient to solve numerically a $3 + 2$ differential-algebraic system of equations.

7.3 Double Track Race Car Model

After a bit of work, we are now ready to set up the fundamental governing equations for the *transient* handling of a race car equipped with *limited-slip differential* and with *aerodynamic devices*

$$\begin{aligned}
m(\dot{u} - vr) &= X(u, v, r, \dot{u}, \dot{v}, \dot{r}, \Delta\hat{\omega}, N_X; \omega_h, \delta_v) \\
m(\dot{v} + ur) &= Y(u, v, r, \dot{u}, \dot{v}, \dot{r}, \Delta\hat{\omega}, N_X; \omega_h, \delta_v) \\
J_z\dot{r} &= N_X + N_Y(u, v, r, \dot{u}, \dot{v}, \dot{r}, \Delta\hat{\omega}, N_X; \omega_h, \delta_v) \\
N_X &= \frac{t_1}{2}\left[F_{y_{11}}\sin(\delta_{11}) - F_{y_{12}}\sin(\delta_{12})\right] + \frac{t_2}{2}\left(F_{x_{22}} - F_{x_{21}}\right) \\
F_{x_{22}} &= \eta_h^{\left(\frac{\arctan(\chi\,\Delta\hat{\omega})}{\pi/2}\right)} F_{x_{21}}
\end{aligned} \tag{7.30}$$

As already stated, a fairly practical way to set up the problem is to assign the angular speed $\omega_h(t)$ of the housing of the differential (Sect. 3.14) and the angular position $\delta_v(t)$ of the steering wheel, and then solve numerically this system of *five* differential-algebraic equations in the five unknown functions $(u(t), v(t), r(t), \Delta\hat{\omega}(t), N_X(t))$. Imposing $\omega_h(t)$ is more realistic than imposing directly the forward speed $u(t)$.

We say it is a system of differential and algebraic equations because there are no derivatives of $\Delta\hat{\omega}(t)$ and $N_X(t)$).

The model (7.30) for race cars is a generalization of the model for road cars presented in Chap. 6. Wings make the vertical loads strongly dependent on the vehicle speed. The limited-slip differential provides a yawing moment very sensitive to the lateral acceleration and to the steer angle. None of these phenomena can be found in (most) road cars. On the other hand, torque vectoring can be activated in modern road cars, whereas any driving aid system is usually prohibited in competitions.

The comparison of (7.30) with (6.34), that is with the governing equation of a double track model for road vehicles, clearly shows the increased complexity of the model. But this is no surprise: a race car exhibits indeed a much richer handling behavior.

7.3.1 Single Track?

A question that naturally arises at this point is whether we can go "single track" or not, as has been done for road cars in Sect. 6.5. To answer this question we should recall that by single track [1–3, 7, 12] we meant a vehicle model having two axle characteristics (6.69), that is two constitutive equations $Y_i(\alpha_i)$, one per each axle, involving only a single kinematic variable each (namely, the axle apparent slip angle).

With limited-slip differentials, this is no longer possible, nor even for the front axle, since there is a strong interaction between lateral and longitudinal tire forces. More precisely, the analysis developed in Sect. 6.5.10 about the role of lateral acceleration

is no longer applicable. Therefore, in this case we cannot end up with a single track model. We have to stick to the more general double track model. However, this is somehow good news, as the double track model is much more realistic, and only a little more complex, than the single track model.

Actually, a sort of *generalized single track* model can still be formulated provided, as it was for road cars:

1. the car has parallel steering ($\varepsilon_1 = 0$);
2. the car has open differential ($\eta_h = 1$) and hence $\Delta X_2 = 0$;
3. it is assumed $\Delta X_1 = 0$.

The important difference with respect to the classical single track model is that, owing to the aerodynamic devices, the axle characteristics are functions also of the forward velocity u, that is $Y_1 = Y_1(\alpha_1, u)$ and $Y_2 = Y_2(\alpha_1, u)$. This is clearly due to the aerodynamic downforces.

7.4 Basics for Steady-State Handling Analysis

It is customary in vehicle dynamics to start with the steady-state analysis, that is with all time-derivatives in the governing equations (7.30) set equal to zero. That means having the vehicle go round along a circle of constant radius at constant forward speed. In practice, it is much more convenient to do a *slowly increasing steer* maneuver, also called *constant speed, variable steer* test. The vehicle is almost in steady-state conditions, but the test procedure is much faster.

Pretty much like in Sect. 6.7, everything is based on the steady-state maps

$$\rho = \frac{r}{u} = \rho(\delta_v, \tilde{a}_y) \qquad \text{and} \qquad \beta = \frac{v}{u} = \beta(\delta_v, \tilde{a}_y) \tag{7.31}$$

which, beside being important by themselves, make also possible to unambiguously define the *gradients*

$$\begin{aligned} \text{grad } \rho &= \left(\frac{\partial \rho}{\partial \tilde{a}_y}, \frac{\partial \rho}{\partial \delta_v} \right) = (\rho_y, \rho_\delta) \\ \text{grad } \beta &= \left(\frac{\partial \beta}{\partial \tilde{a}_y}, \frac{\partial \beta}{\partial \delta_v} \right) = (\beta_y, \beta_\delta) \end{aligned} \tag{7.31'}$$

All these quantities are well defined in any vehicle, including race cars.

The new global approach to handling evaluation, called MAP, introduced in Sect. 6.8, turns out to be very informative for race cars as well, as will be shown shortly. The analysis will be particularly interesting when aerodynamics is taken into account.

In (7.31) we have omitted, with respect to (6.98) and (6.111), the r.h.s. terms, that is those involving the apparent slip angles α_1 and α_2 (6.53) and the steering

angles. This has been done for greater generality, because α_1 and α_2 are not well defined, unless we assume $\varepsilon_1 = \varepsilon_2 = 0$,[3] as in (6.49). But the key point is that α_1 and α_2, even if well defined, are no longer functions of the lateral acceleration $\tilde{a}_y$ only. This aspect has a lot of important consequences. For instance, the classical handling diagram [8–10] does not exist any more. As will be shown in the next section, it has to be replaced by the *handling surface*, first introduced in [4–6].

7.5 The Handling Diagram Becomes the Handling Surface

Although, in our opinion, the handling surface has been superseded by the MAP approach, it still deserves to be explained.

The well known handling diagram, discussed in Sect. 6.7.4, is made up of the handling curve and a straight line (Fig. 6.28).

As already stated in Sect. 6.7.4, this is quite a fortunate coincidence. In general, the *handling curve* must be replaced by the *handling surface*. Indeed, any steady-state configuration depends on *two* parameters (as a minimum), like, e.g., the forward speed u and the steering angle δ_v. In vehicles with open differential and no wings, it happens that some quantities depend only on one parameter, namely the lateral acceleration $\tilde{a}_y$. Therefore, the handling surface becomes a cylinder, whose projection is the handling curve, as shown in [5]. Let us elaborate this concept in detail.

7.5.1 Handling with Locked Differential (and No Wings)

Before dealing with the handling of race cars with significant aerodynamic downforces, we address the effect of the locked differential alone, with respect to the open differential. To do this, we consider road cars, which have very little, if any, aerodynamic vertical forces (no wings and not too high speed).

7.5.1.1 Steady State

According to the classical theory, we perform a number of (almost) steady-state tests, like slowly increasing steer manoeuvres, first for a vehicle with open differential, and then for the same vehicle but with a locked differential.

In all cases we monitor the forward speed u, the lateral speed v (or, equivalently, the vehicle slip angle $\beta = v/u$), the yaw rate r, the steering wheel angle δ_v. Although not strictly necessary, it is very convenient to monitor directly also the lateral acceleration $\tilde{a}_y = ur$. We also know the gear ratios of the steering system. Assuming, as in (6.49),

[3] However, many race cars do have $\varepsilon_1 = \varepsilon_2 = 0$, that is parallel steering.

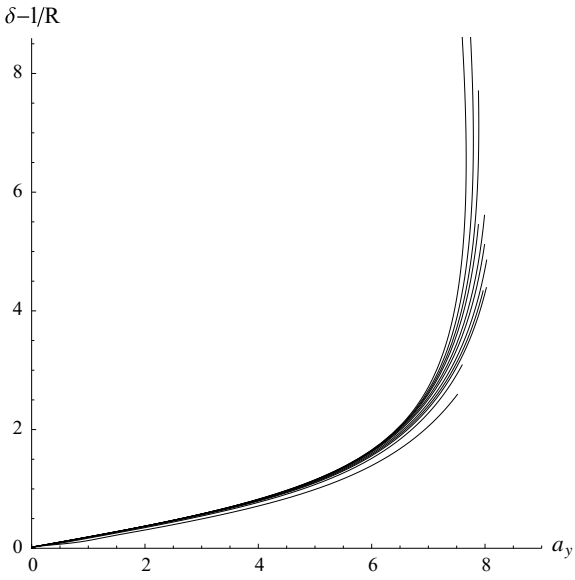

Fig. 7.11 Vehicle with *open* differential: handling curve(s) obtained in constant speed, variable steer tests

$\varepsilon_1 = \varepsilon_2 = 0$, we can define the front steer angle $\delta_1 = \tau_1 \delta_v$ and the rear steer angle $\delta_2 = \tau_2 \delta_v$. The last useful piece of information is the wheelbase $l = a_1 + a_2$.[4]

The classical handling curve is the plot of $(\delta_1 - \delta_2) - l/R = \delta - l/R$ versus $\tilde{a}_y$, as discussed in Sect. 6.7.4. An understeer vehicle with *open* differential has a handling diagram like in Fig. 7.11: we get about the same curve, as function of $\tilde{a}_y$, regardless of the combination of forward speed and steer angles. On the other hand, performing constant speed, variable steer tests on the same vehicle, but with *locked differential*, yields *a different handling curve for each forward speed*, as shown in Fig. 7.12.

The framework to understand what is going on in these cases is the *handling surface*, that is the plot of

$$\delta - \frac{l}{R} = f\left(\tilde{a}_y, \frac{l}{R}\right) \tag{7.32}$$

which is no longer a function of $\tilde{a}_y$ only, but needs another variable, like, e.g., l/R. Indeed, since there are two input quantities, like the forward speed and the steer angle, it is normal to have to deal with two variables at steady-state. The handling curves are just the *projections* of some *sections* of the handling surface onto the plane $(\tilde{a}_y,\ \delta - l/R)$.

It happens that the handling surface is almost a cylinder for the open differential case, as shown in Fig. 7.13. Therefore, it always collapses into almost a single curve when projected. But more general vehicles (or better, less peculiar vehicles), that is all vehicles with at least one of the following features:

[4] Actually, vehicle dynamics had better avoid using the wheelbase, as discussed in Sect. 6.9.

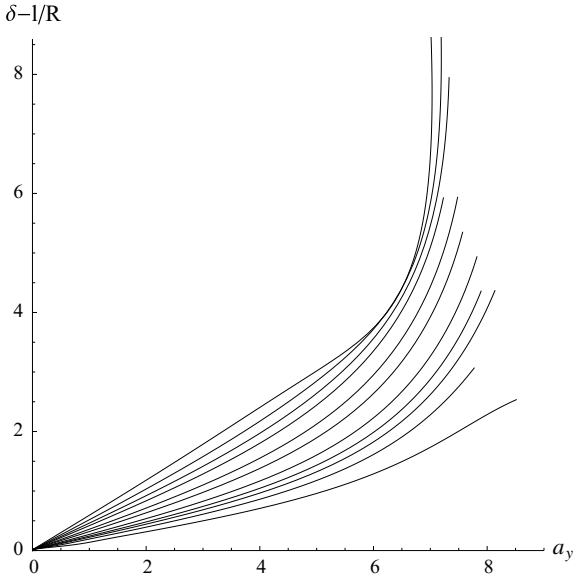

Fig. 7.12 Vehicle with *locked* differential: handling curves obtained in constant speed, variable steer tests

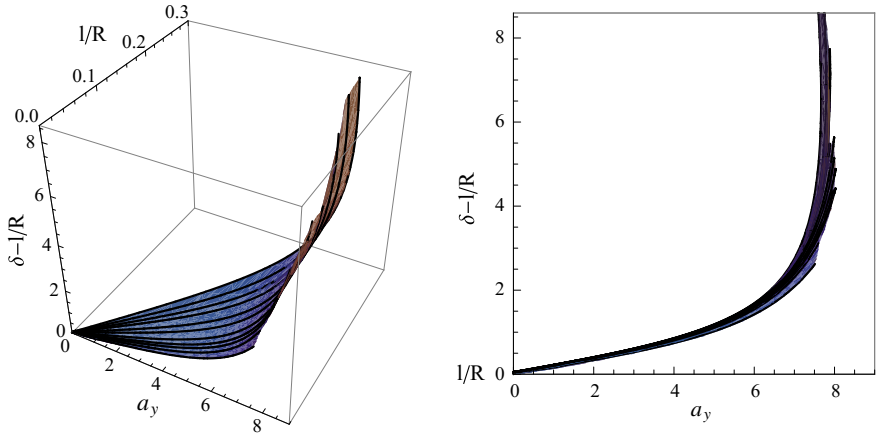

Fig. 7.13 Cylindrical handling surface for a vehicle with *open* differential

- locked differential;
- limited-slip differential;
- aerodynamic wings;
- more than two axles;
- large steer angles;

they all exhibit a non-cylindrical handling surface, like the one shown in Fig. 7.14.

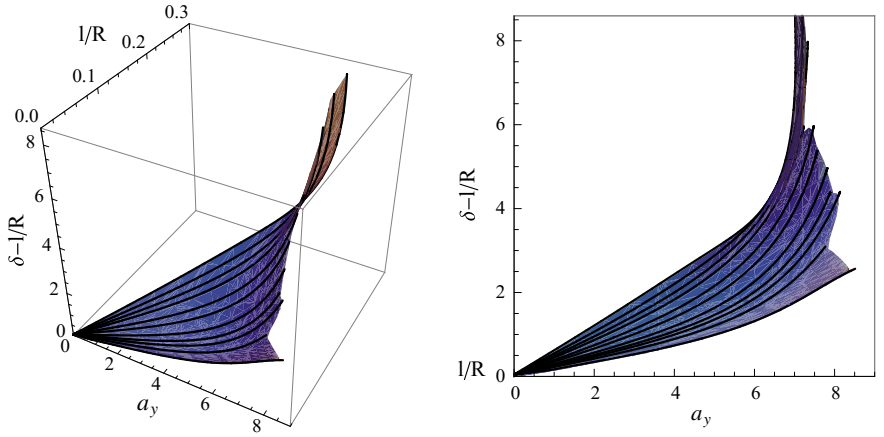

Fig. 7.14 Non-cylindrical handling surface for a vehicle with *locked* differential

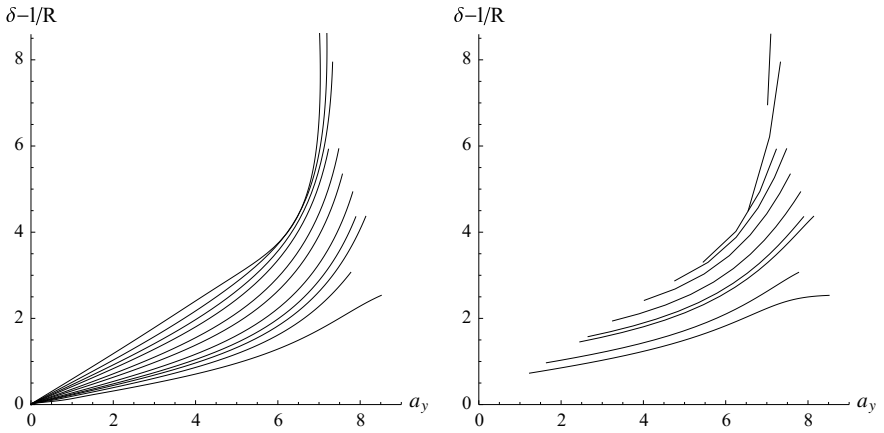

Fig. 7.15 Vehicle with *locked* differential: comparison between handling curves obtained in constant speed, variable steer tests (left) and constant steer, variable speed tests (right)

Therefore, drawing handling curves can be very confusing for a vehicle with locked differential, as the kind of test matters a lot. For instance, constant steer, variable speed tests yield curves that are totally different with respect to the constant speed, variable steer tests, as shown in Fig. 7.15. They are, however, just different sections of the very same handling surface. Again, if the differential is open, the handling surface is cylindrical, and all tests, that is all sections, project onto about the same curve, as shown in Fig. 7.16, regardless of the kind of maneuver.

To elaborate this idea further, we present Figs. 7.17 and 7.18 taken from [5]. The first Figure shows sections of the handling surface for several values of the constant speed u. In the plane $(l/R, \tilde{a}_y) = (lr/u, ur)$, they appear as straight lines from the

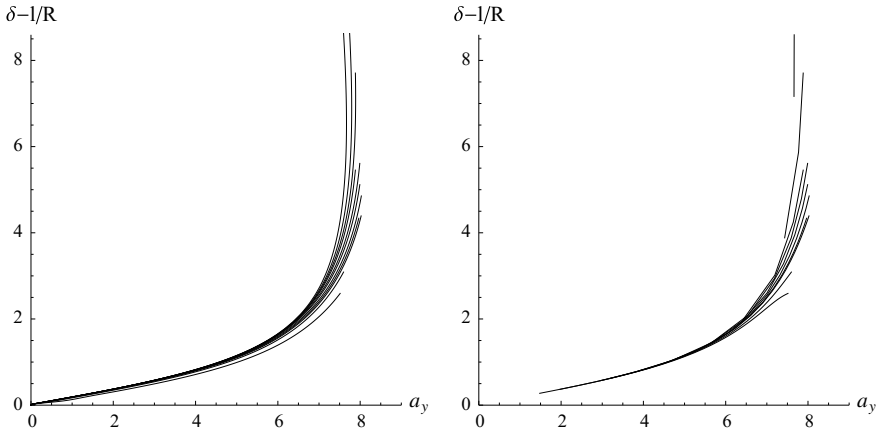

Fig. 7.16 Vehicle with *open* differential: comparison between handling curves obtained in constant speed, variable steer tests (left) and constant steer, variable speed tests (right)

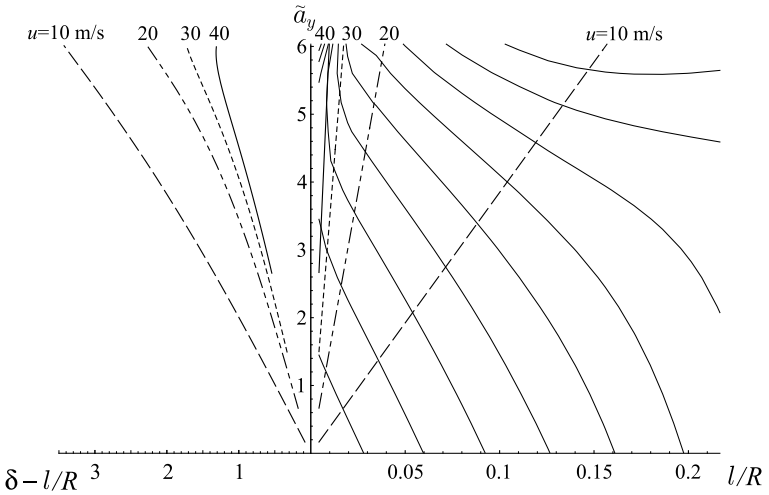

Fig. 7.17 Handling curves at constant speed (left) as sections of the handling surface (right) [5]

origin. The projections of each of these sections in the plane $(\tilde{a}_y, \delta - l/R)$ are shown in the left part. Similarly, the second Figure shows sections of the handling surface for several values of the constant radius R. In the plane $(l/R, \tilde{a}_y)$, they appear as vertical straight lines. The projections of each of these sections in the plane $(\tilde{a}_y, \delta - l/R)$ are shown in the left part.

At low speed, like $u = 9$ m/s, and large steer angle $\delta_1 = 18°$, an ordinary road car receives from the road, more or less, the forces depicted in Fig. 7.19 when equipped with an open differential, and the forces shown in Fig. 7.20 when equipped with a locked differential. Also shown, in Fig. 7.21, is the case of a limited-slip differential

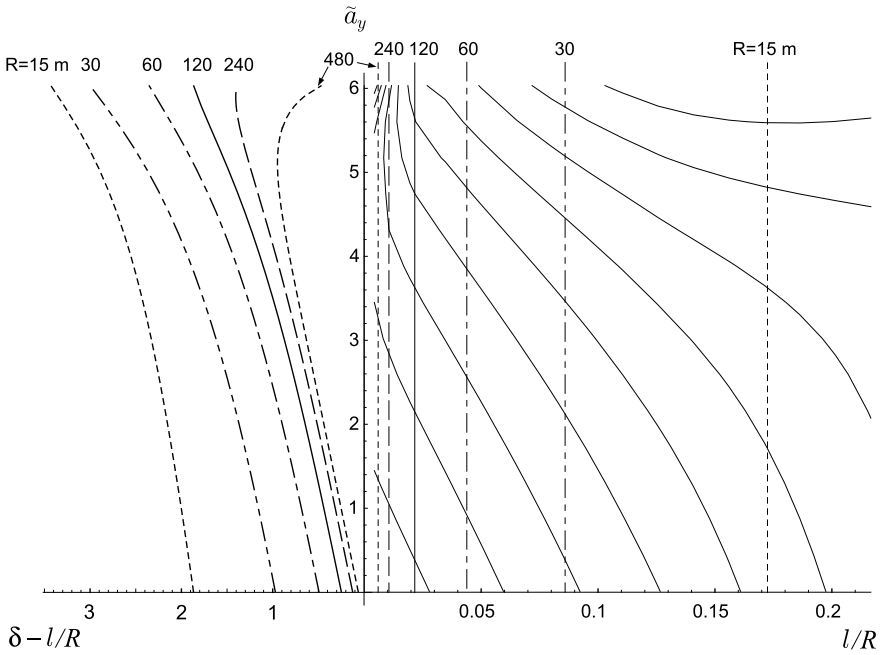

Fig. 7.18 Handling curves at constant turning radius (left) as sections of the handling surface (right) [5]

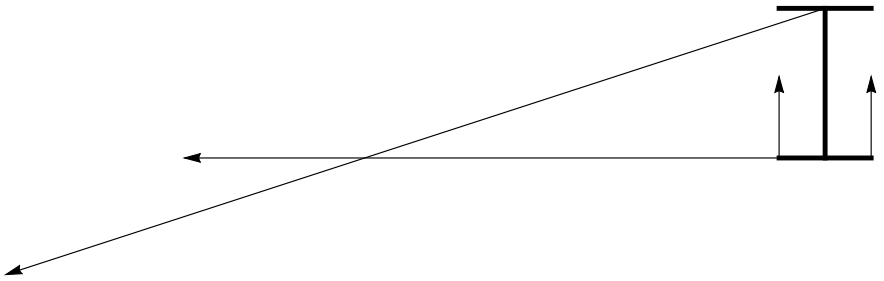

Fig. 7.19 Vehicle with open differential: forces received from the road at $u = 9$ m/s and $\delta_1 = 18°$

with internal efficiency $\eta_h = 0.33$. Similar figures can be found in Sect. 3.14. The three cases are deeply different. The yawing moment of the two longitudinal forces is obviously zero with open differential. With locked differential, at such low speed and high steer angle, the external wheel provides a braking force, which must be counteracted by the inner wheel: the yawing moment is so high to affect significantly both front and rear lateral forces. The limited-slip case is something in between, with a small yawing moment coming from the longitudinal forces.

At much higher speed, say $u = 54$ m/s, and low steer angle, say $\delta_1 = 3°$, the moment due to the locked differential changes sign, as shown in Fig. 7.22. This is a typical and important phenomenon, due to the lateral load transfer. The inner wheel

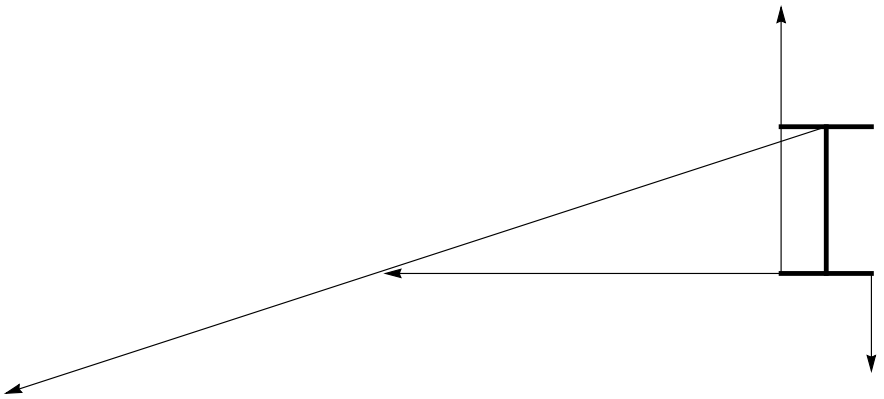

Fig. 7.20 Vehicle with locked differential: forces received from the road at $u = 9$ m/s and $\delta_1 = 18°$

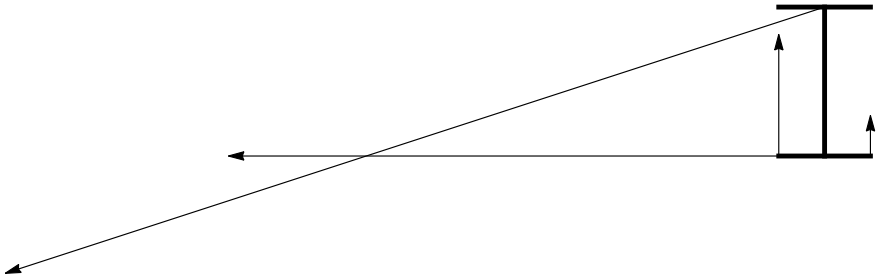

Fig. 7.21 Vehicle with limited-slip differential ($\eta_h = 0.33$): forces received from the road at $u = 9$ m/s and $\delta_1 = 18°$

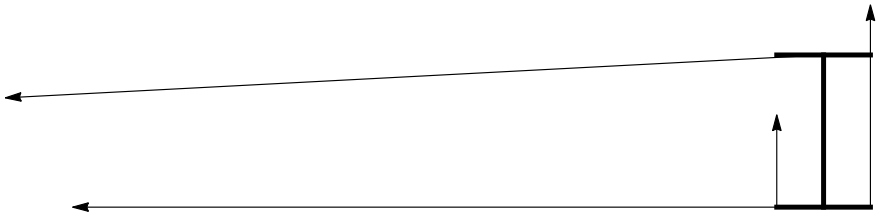

Fig. 7.22 Vehicle with locked differential: forces received from the road at $u = 54$ m/s and $\delta_1 = 3°$

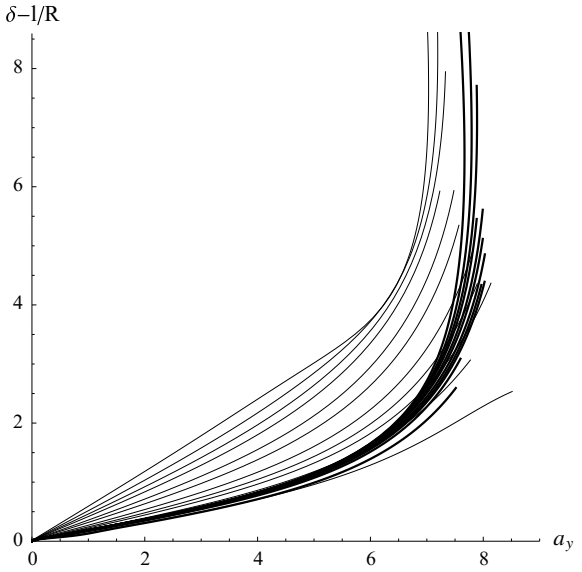

Fig. 7.23 Handling curves obtained in constant speed, variable steer tests: comparison between locked differential (thin lines) and open differential (thick lines)

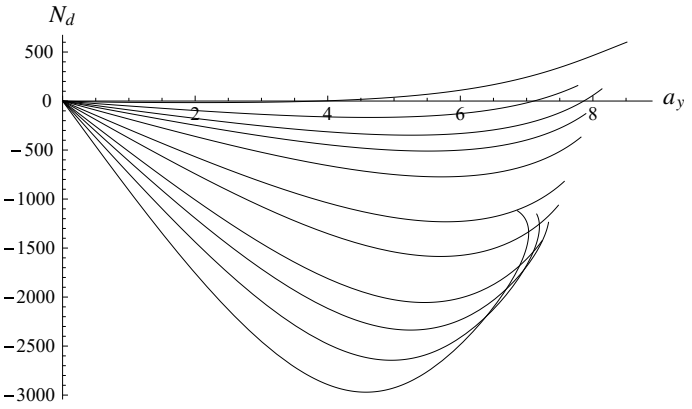

Fig. 7.24 Locked differential: yawing moment versus lateral acceleration for several speeds

barely touches the ground and cannot provide much longitudinal force, thus limiting, with an open differential, the external force as well.

Superimposing the handling curves obtained in constant speed, variable steer tests for both open and locked differential, as shown in Fig. 7.23, we can appreciate the understeer effect at low lateral acceleration and the oversteer effect at high lateral acceleration. This is due to the yawing moment N_d, which has the typical behavior shown in Figs. 7.24 and 7.25 in case of locked differential. Of course, N_d is equal to zero when the differential is open.

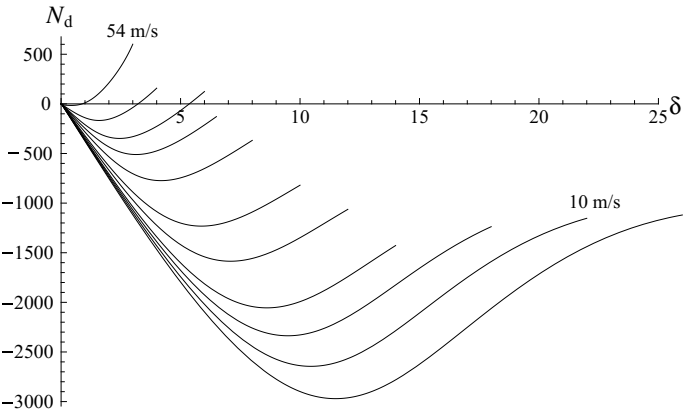

Fig. 7.25 Locked differential: yawing moment versus steer angle for several speeds

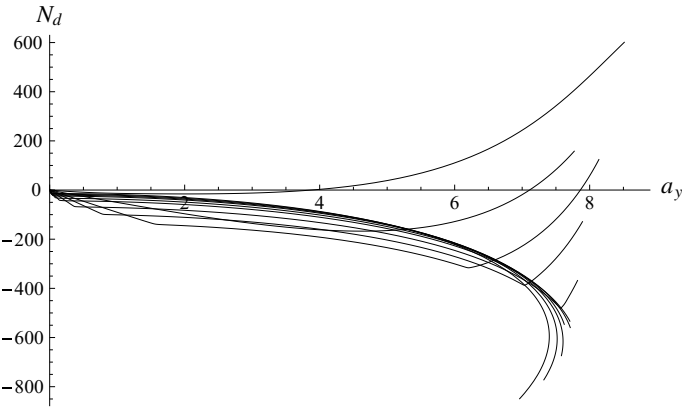

Fig. 7.26 Limited slip differential ($\eta_h = 0.33$): yawing moment versus lateral acceleration for several speeds

In case of limited-slip differential with $\eta_h = 0.33$, the yawing moment N_d due to the longitudinal forces is something like in Figs. 7.26 and 7.27. It is worth noting the "knee" in some curves due to the internal wheel switching from slow wheel to fast wheel.

7.5.1.2 Power-Off and Power-On

When braking using the engine, that is in *power-off* conditions, while negotiating a curve, the longitudinal forces are like in Fig. 7.28 in case of locked or limited-slip

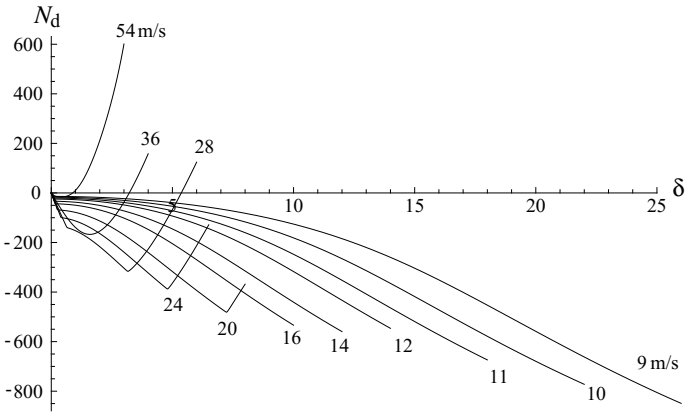

Fig. 7.27 Limited slip differential ($\eta_h = 0.33$): yawing moment versus steer angle for several speeds

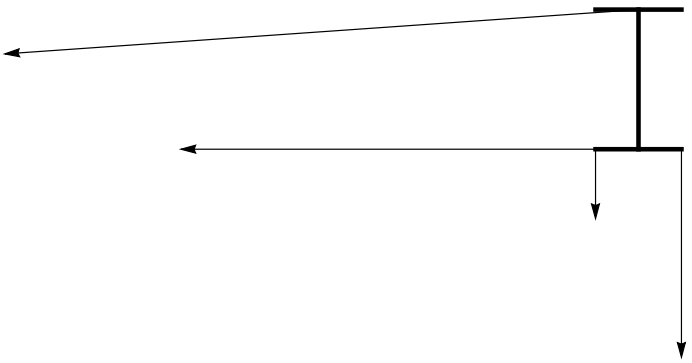

Fig. 7.28 Vehicle with locked or limited-slip differential: forces received from the road during power-off

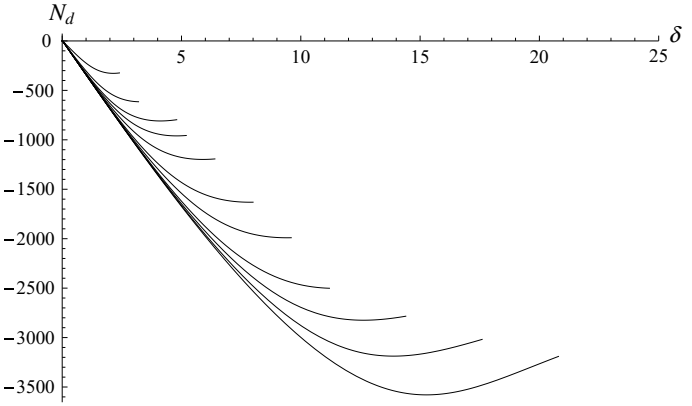

Fig. 7.29 Locked differential: yawing moment versus steer angle for several speeds during power-off

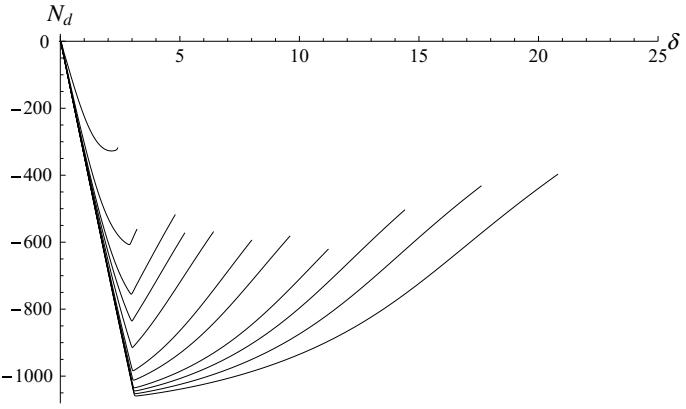

Fig. 7.30 Limited slip differential ($\eta_h = 0.33$): yawing moment versus steer angle for several speeds during power-off

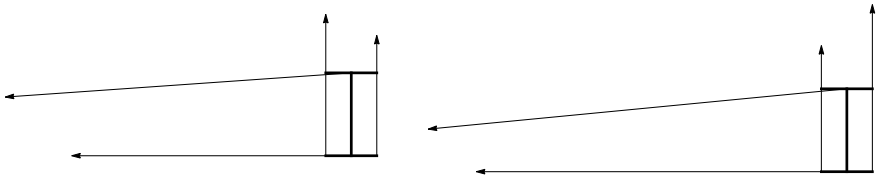

Fig. 7.31 Vehicle with locked or limited-slip differential: forces received from the road during power-on

differential. The corresponding yawing moments N_d are plotted in Figs. 7.29 and 7.30 versus the steer angle $\delta = \delta_1 - \delta_2$, for several values of the forward speed.

While during power-off it is always the external wheel that receives the highest (braking) longitudinal force, as shown in Fig. 7.28, under *power-on* conditions, while negotiating a curve with a vehicle with locked differential, there can be two possible cases, depending on the value of the lateral acceleration a_y (Fig. 7.31). This is better understood looking at the plot of N_d as a function of the lateral acceleration a_y, as shown in Fig. 7.32 for locked differential, and in Fig. 7.33 for limited-slip differential, in both cases for several values of the forward speed u (ranging from 9 m/s up to 54 m/s): the moment can either be negative or positive, whereas in Figs. 7.29 and 7.30 it is always negative.

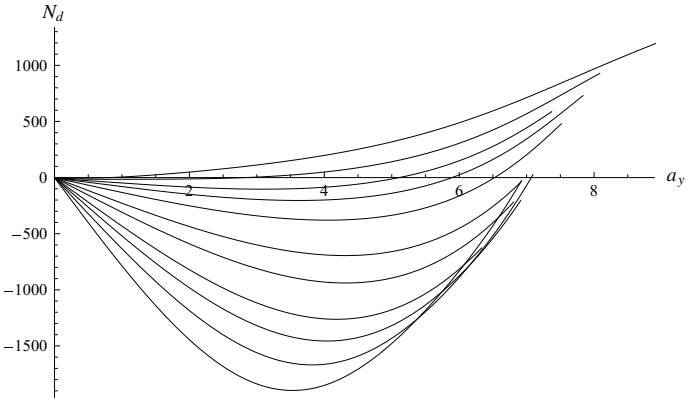

Fig. 7.32 Locked differential: yawing moment versus lateral acceleration for several speeds during power-on

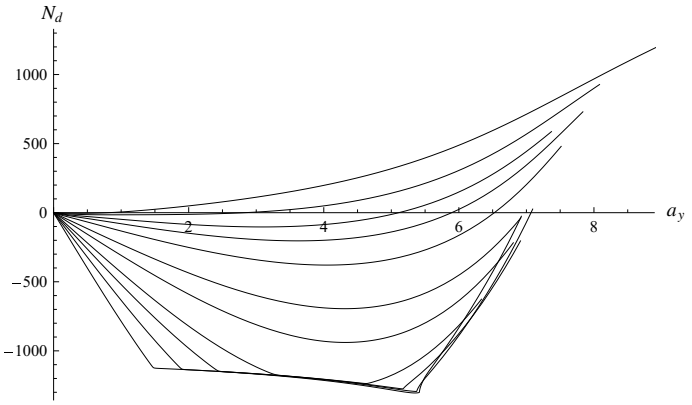

Fig. 7.33 Limited slip differential ($\eta_h = 0.33$): yawing moment versus lateral acceleration for several speeds during power-on

Although they are the main topic of the next section, we show the MAPs for the power-off and power-on cases of a road car. This new global approach has been already introduced and described in detail in Sect. 6.8 for steady-state handling analysis of road cars. The maps ρ–δ for locked differential are shown in Fig. 7.34, while the same maps for open differential are given in Fig. 7.35. The oversteer effect of power-on for a rear-wheel-drive car is evident in both cases. However, the locked differential makes this phenomenon stronger.

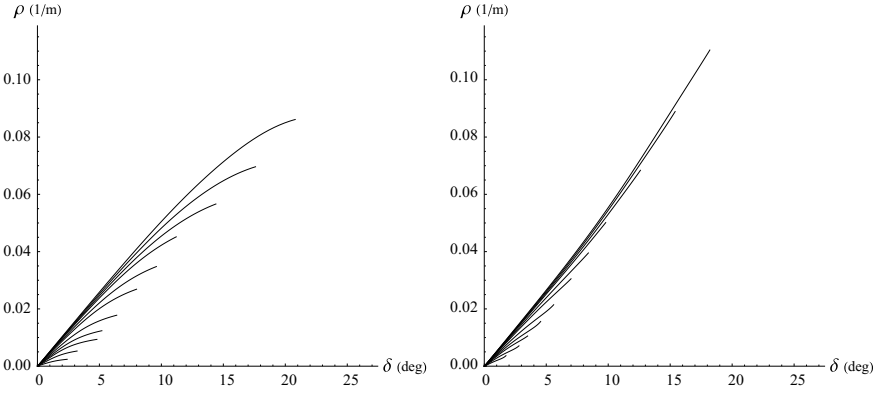

Fig. 7.34 Lines at constant speed u in the handling map ρ–δ during power-off (left) and power-on (right) for a road vehicle with *locked* differential

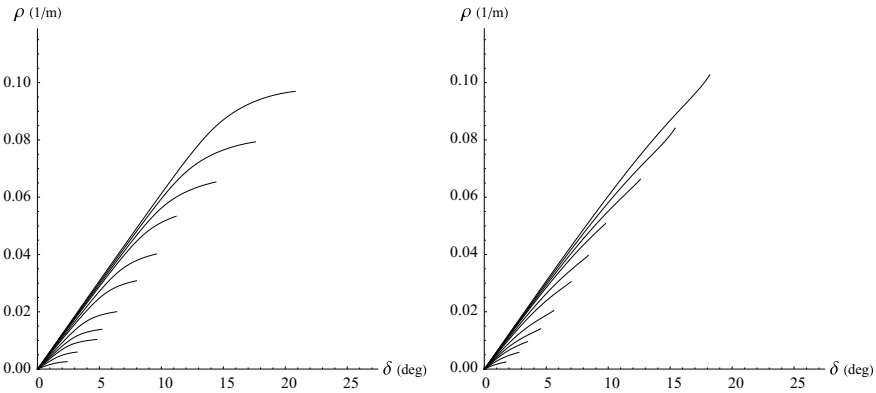

Fig. 7.35 Line at constant speed u in the handling map ρ–δ during power-off (left) and power-on (right) for a road vehicle with *open* differential

The maps β–ρ for power-off and power-on for a vehicle equipped with a locked differential are shown in Fig. 7.36. Again, the lines at constant steer angle clearly show, and do it in a quantitative way, the oversteer effect of power-on. For comparison, the same maps for a vehicle with open differential are given in Fig. 7.37.

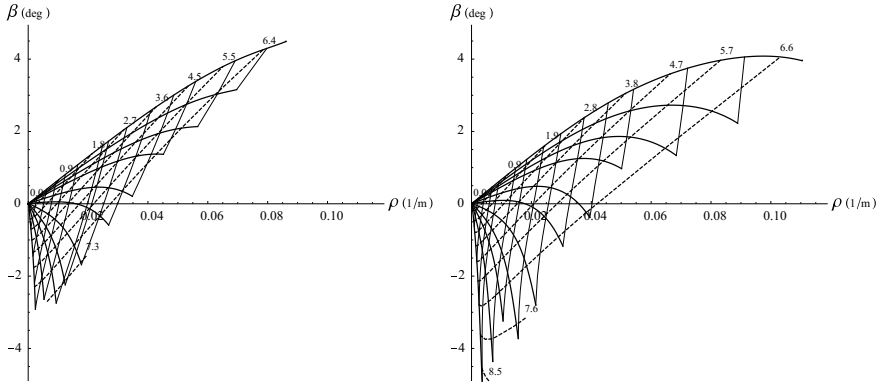

Fig. 7.36 Handling map β–ρ during power-off (left) and power-on (right) for a road vehicle with *locked* differential (constant u: solid thick lines, constant δ: thin solid lines, constant a_y: dashed lines)

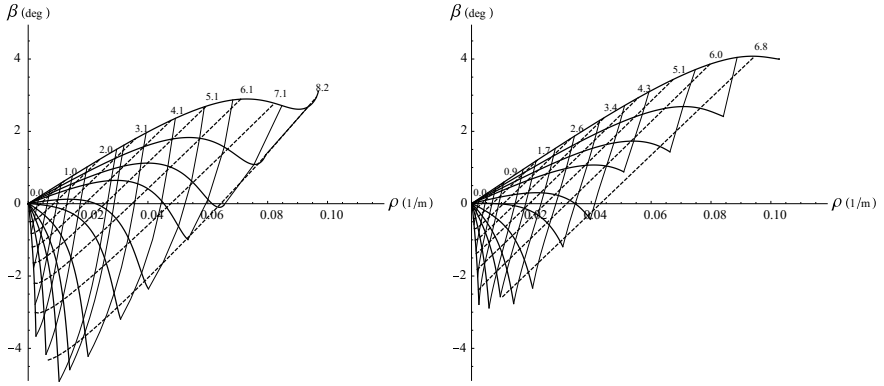

Fig. 7.37 Handling map β–ρ during power-off (left) and power-on (right) for a road vehicle with *open* differential (constant u: solid thick lines, constant δ: thin solid lines, constant a_y: dashed lines)

7.6 Handling of Formula Cars

It is in the handling of Formula Cars that aerodynamics comes really into play (Fig. 7.9). Thanks to well designed aerodynamic devices, very high downforces are generated at high speeds, although at the price of high drag as well. A mathematical model that takes aerodynamics into account has been developed in Sect. 7.1. Here we discuss some of the main phenomena that make the handling of this kind of cars so peculiar. We start with the handling surface to move on to the Maps of Achievable Performance (MAP's), first at steady state, and then during power-off and power-on.

Although these cars have a limited-slip differential, at the center of a bend, that is when the vehicle is more or less close to steady state, the differential is basically open.

Therefore, the steady-state analysis is more realistic if done with open differential, leaving the locked one for power-off and power-on. In all cases we consider speeds in the range 20–80 m/s.

7.6.1 Handling Surface

The handling surface has been introduced and discussed in Sect. 7.5. It is the plot of $\delta - l/r$ as a function of the lateral acceleration $\tilde{a}_y$ and the ratio $l/R = l\rho$. In case of significant aerodynamic effects, it is not cylindrical. This geometric feature is the counterpart of a very practical and obvious phenomenon: the speed matters a lot when a car is making a turn. The faster the car, the higher the lateral acceleration that can be achieved, assuming the same physical grip between the tires and the road. Therefore, once again, if we try to get the classical handling curve we will end up with a number of different handling curves, one for each testing condition. Tests at constant speed and variable steer will yield a different curve for each speed. Tests at constant steer and variable speed will produce a different set of curves, and so on.

These aspects are better understood looking at Fig. 7.38, which shows the handling curves for a Formula car with open differential as obtained in constant speed, slowly variable steer tests. It is evident that the higher the speed, the higher the lateral acceleration.

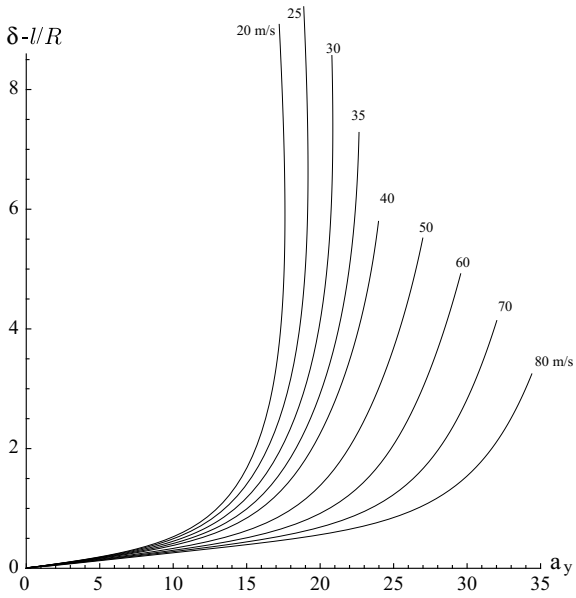

Fig. 7.38 Formula car with *open* differential: different handling curves obtained in constant speed, variable steer tests

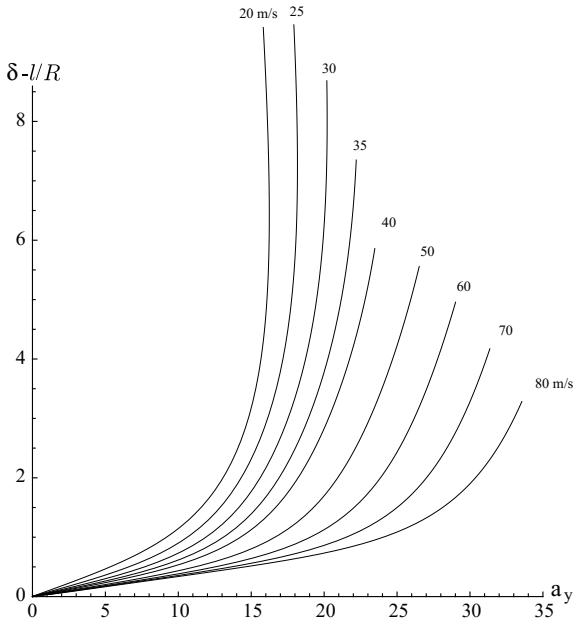

Fig. 7.39 Formula car with *locked* differential: different handling curves obtained in constant speed, variable steer tests

Locking completely the differential affects these handling curves, but not much, as shown in Fig. 7.39 (the aerodynamics is more influential). The main difference is, perhaps, that all curves in case of open differential share the same slope near the origin of the reference system, whereas in case of locked differential each one has a different slope, even when $\tilde{a}_y \simeq 0$.

As expected, performing constant steer, slowly variable speed tests yield different handling curves, as shown in Fig. 7.40. However, all these curves are just the projections of some sections of the *handling surface*, as shown in Fig. 7.41.

7.6.2 Map of Achievable Performance (MAP)

The global approach MAP has been introduced in Sect. 6.8. The emphasis there was on road cars, that is cars without any significant aerodynamic downforces and with open differential. However, this new approach is completely general, and its application to race cars is straightforward. More precisely, MAPs for road cars and race cars are qualitatively the same, differing only quantitatively.

The basic idea, as discussed on p. 262, is to employ the maps

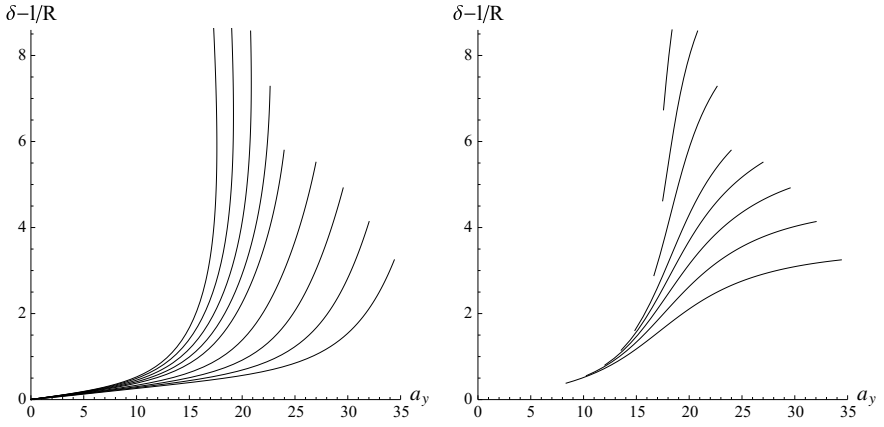

Fig. 7.40 Formula car with *open* differential: comparison between handling curves obtained in constant speed, variable steer tests (left) and constant steer, variable speed tests (right)

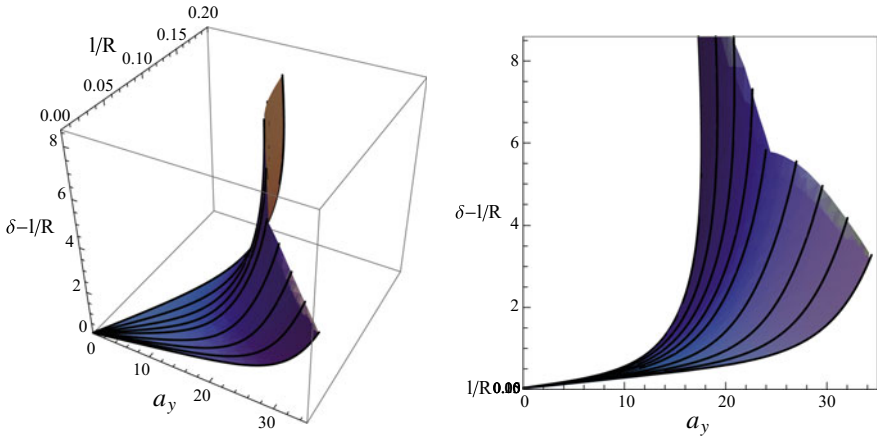

Fig. 7.41 Non-cylindrical handling surface for a Formula car with *open* differential

$$\begin{aligned}\rho &= \rho(\delta, u) = \frac{\delta}{l} - \frac{\alpha_1(\delta, u) - \alpha_2(\delta, u)}{l} \\ \beta &= \beta(\delta, u) = \left(\frac{(1+\hat{\chi})a_2 + \hat{\chi}a_1}{l}\right)\delta - \frac{\alpha_1(\delta, u)a_2 + \alpha_2(\delta, u)a_1}{l}\end{aligned} \tag{6.114'}$$

as functions of two variables to monitor the vehicle at steady state. This is a more general point of view than the handling surface (not to mention the handling diagram).

The maps in this section are typical for a Formula 1 car, year 2013. As usual, all quantities are in SI units, except angles that are in degrees.

7.6.2.1 ρ–δ MAP (Curvature-Steer Angle)

The first map to be considered is the curvature $\rho = r/u$ versus the wheel steer angle δ (although we could employ the steering wheel angle δ_v as well). In Fig. 7.42 we can see the lines at constant speed u, ranging from 20 to 80 m/s, and also the lines at constant lateral acceleration $\tilde{a}_y$, in case of open differential. In Fig. 7.43, we have the same picture, but for locked differential.

Lines at constant speed for open and locked differential are compared in Fig. 7.44. As expected, the locked differential makes the car turn on bigger radiuses (hence smaller values of ρ).

The strong influence of aerodynamics on the handling of the vehicle is highlighted by the pattern of the lines at constant lateral acceleration. Going back to Fig. 6.44, that is to the map for an ordinary road vehicle, we see that each line at constant $\tilde{a}_y$ intersects all lines at constant u. That means that the level of lateral acceleration that can be achieved is not affected by the forward speed (no wings). On the other hand, in Figs. 7.42 and 7.43, only lines up to about 16 m/s^2 intersect all constant speed lines. The lines for $\tilde{a}_y > 16$ m/s^2 only intersect lines for sufficiently high speed. Indeed, 1.6 is about the grip coefficient between the tire and the road, that is the "physical grip". The grip that does not need any aerodynamic contribution. Higher values of apparent grip do indeed need aerodynamic downforce and hence they can be achieved only for sufficiently high values of the forward speed u. The map shows this fact, and does so in a clear and global way. A close-up is shown in Fig. 7.45 for better clarity.

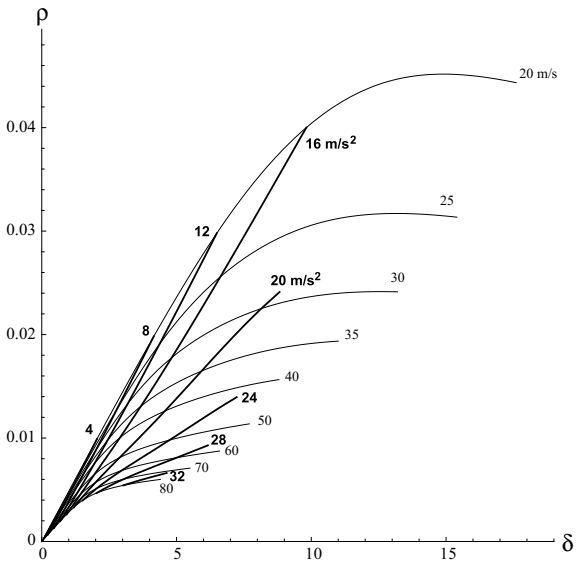

Fig. 7.42 ρ–δ MAP of a *Formula 1* car with *open* differential. Curves at constant speed u and curves at constant lateral acceleration $\tilde{a}_y$

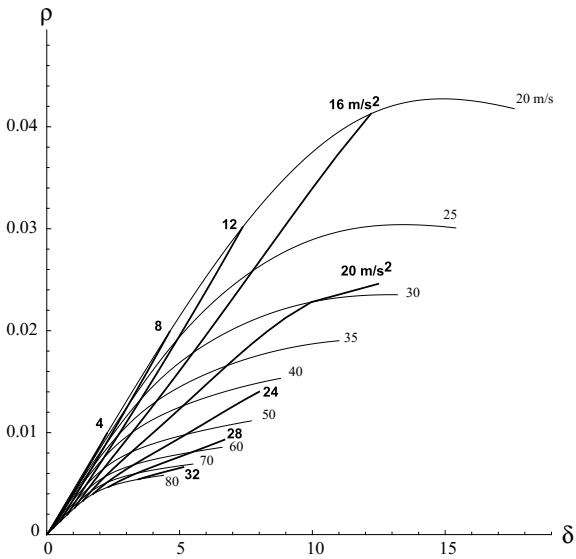

Fig. 7.43 ρ–δ MAP of a *Formula 1* car with *locked* differential. Curves at constant speed u and curves at constant lateral acceleration $\tilde{a}_y$

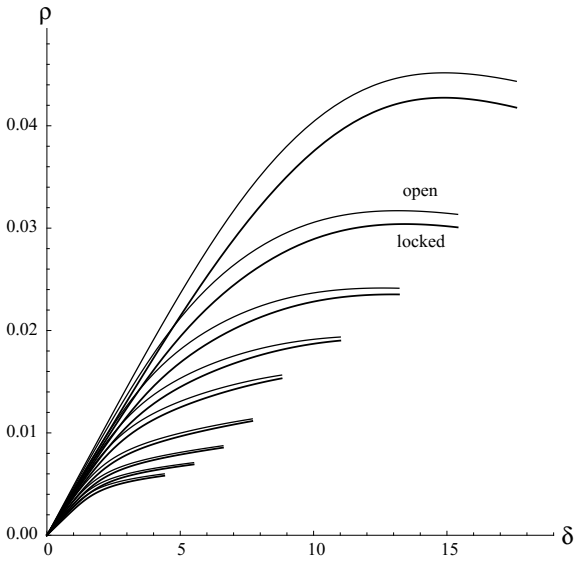

Fig. 7.44 Comparison between Figs. 7.42 and 7.43 for lines at constant speed

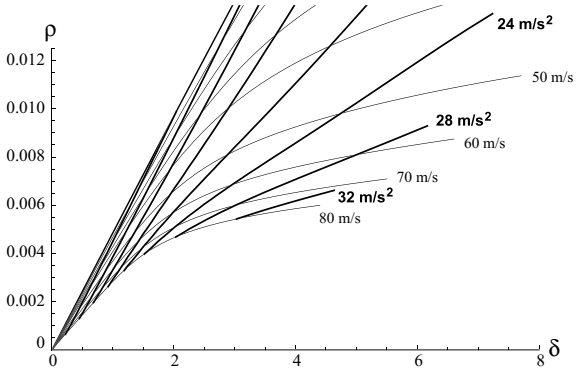

Fig. 7.45 Close-up of Fig. 7.42

7.6.2.2 β–ρ MAP (Vehicle Slip Angle-Curvature)

Also interesting is the handling β–ρ MAP, that is vehicle slip angle versus curvature. The lines at constant speed u and the lines at constant lateral acceleration $\tilde{a}_y$ are shown in Fig. 7.46. Again, only lines for $\tilde{a}_y < 16$ m/s^2 intersect all lines at constant speed, thus indicating that 1.6 is indeed the physical grip (of course we could be more precise by drawing more lines). Therefore, we have a tool to obtain a good approximation of the physical grip.

Also interesting is the overall picture, which shows how the control parameter u and δ are related to curvature and vehicle slip angle. For instance, if $u > 30$ m/s, we have basically $\beta \leq 0$ (in a left turn) at any speed.

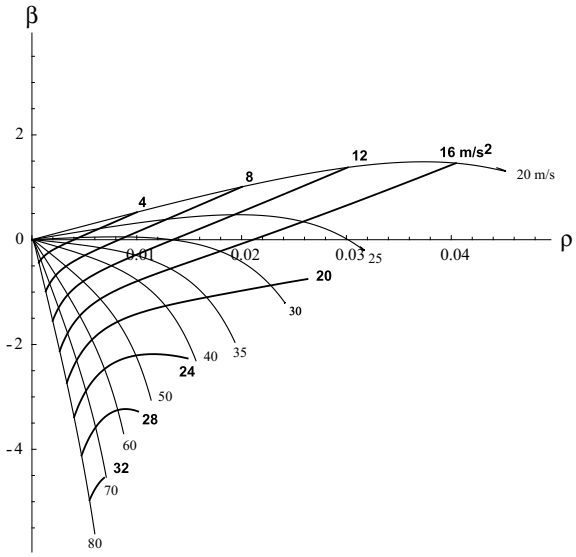

Fig. 7.46 β–ρ MAP for a Formula 1 car with open differential. Curves at constant speed u and curves at constant lateral acceleration $\tilde{a}_y$

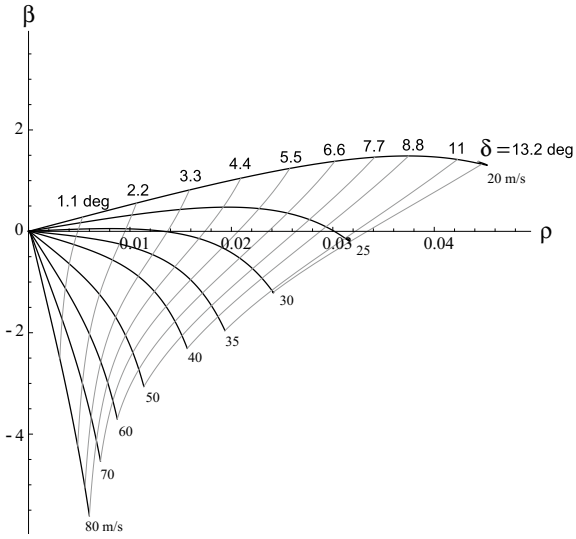

Fig. 7.47 β–ρ MAP or a Formula 1 car with open differential. Curves at constant speed u and curves at constant steer angle δ

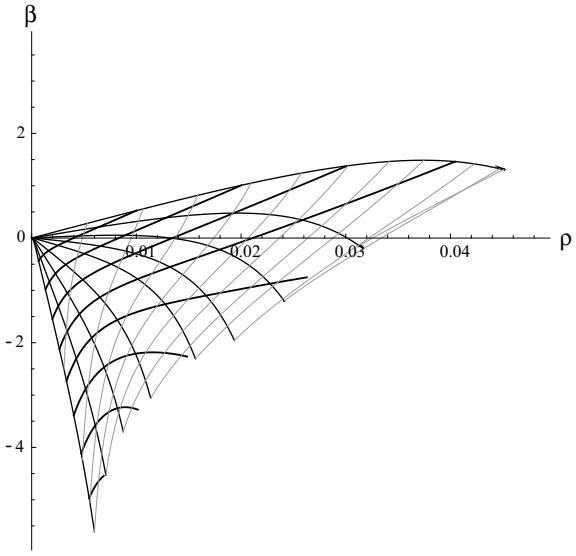

Fig. 7.48 β–ρ MAP for a Formula 1 car with open differential. Superimposition of Figs. 7.46 and 7.47

Lines at constant steer angle are shown in Fig. 7.47. Looking at the slope of these curves, it immediately arises that the vehicle is more understeer at low speeds than at high speeds.

To help the reader catch other features in this map, all lines are shown in Fig. 7.48.

7.6.2.3 Set-Up Identification

Another interesting application of the MAP's is to compare set-ups. This is done in Figs. 7.49 and 7.50 for two set-ups which have different aerodynamic balances. The second set-up (dashed lines) has higher aerodynamic load on the front axle and less aerodynamic load on the rear axle.

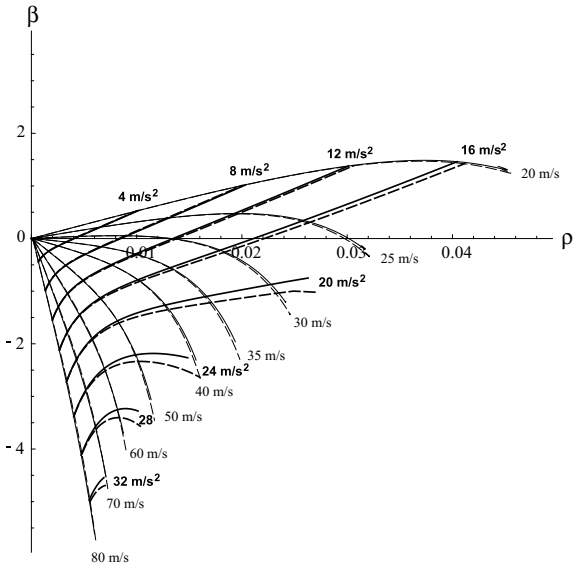

Fig. 7.49 Comparison of curve at constant lateral acceleration for two set-ups with different aerodynamic balance

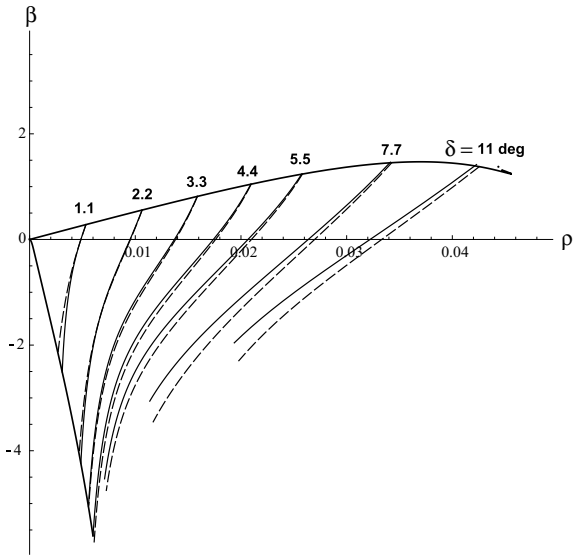

Fig. 7.50 Comparison of curve at constant steer angle for two set-ups with different aerodynamic balance

Very interesting is to observe that the lines at constant $\tilde{a}_y$ that are more affected are precisely those that need aerodynamic downforces to be achieved (Fig. 7.49).

From Fig. 7.50 we see that the new aerodynamic balance does not affect the lines at constant δ in a uniform way. This may help understand which set-up is faster for a given circuit.

7.6.2.4 Power-Off and Power-On

So far we have considered steady-state conditions. However, a Formula car is almost always under transient conditions, with the driver acting on the gas and/or brake pedals. The MAP's can be useful to monitor what is going on also during these more general working conditions. The trick is to do, e.g., constant speed, variable steer simulations as if the car were constantly going uphill or downhill. This way, we have, strictly speaking, steady-state conditions, but the loads on the tires are pretty much like if the car were accelerating or slowing down with the engine (no braking), that is during power-on and power-off conditions.

During power-off and power-on, the differential of a Formula 1 car is locked. Therefore, all Figures in this section are for locked differential.

A few Figures are provided to show how the MAP's can be used to have a global view of the vehicle behavior even under pseudo-transient conditions. Figure 7.51

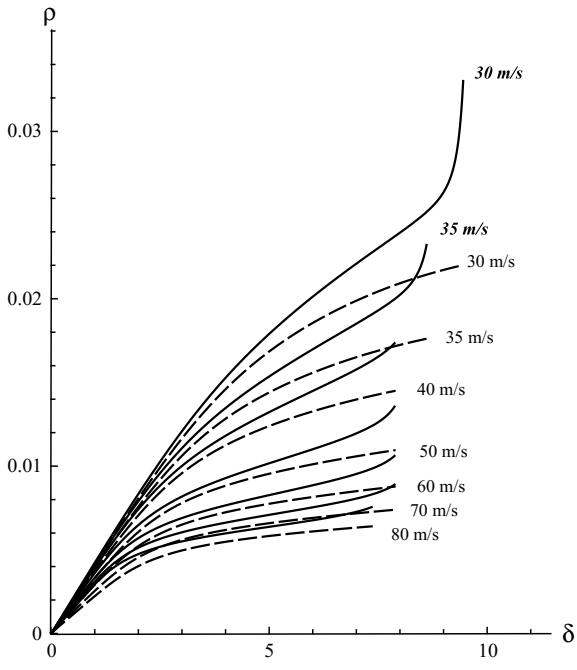

Fig. 7.51 Lines at constant speed in the ρ–δ MAP for a Formula 1 car during power-off (dashed lines) and power-on (solid lines)

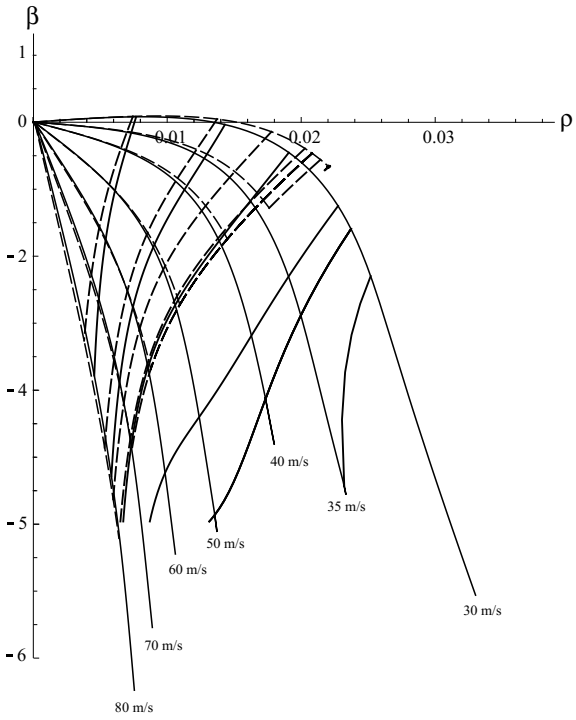

Fig. 7.52 Lines at constant u and constant δ in the β–ρ MAP for a Formula 1 car during power-off (dashed lines) and power-on (solid lines)

shows the ρ–δ map with lines at constant speed during power-off (dashed lines) and power-on (solid lines). Speeds below 30 m/s have been omitted. The two cases are for a longitudinal acceleration of ± 0.5 m/s^2. In Fig. 7.52 there is the comparison of power-off (dashed lines) and power-on (solid lines) in the plane β–ρ. At high steer angles and relatively low speeds there are, as expected, very big differences.

During power-on, the locked differential generates a yawing moment that can have either the same sign as the yaw rate (Fig. 7.53) or opposite sign (Fig. 7.54), depending on the operating conditions of the vehicle.

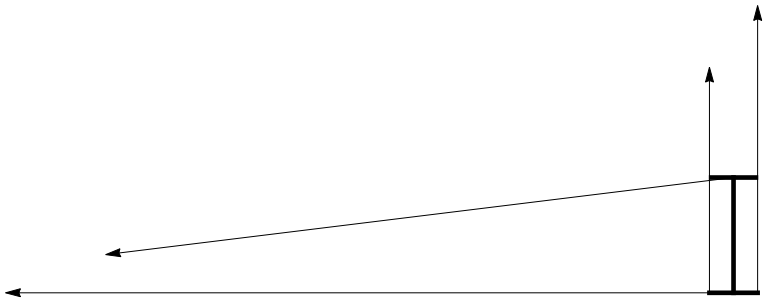

Fig. 7.53 Power-on with locked differential: forces received from the road at $u = 40$ m/s and $\delta = 7°$

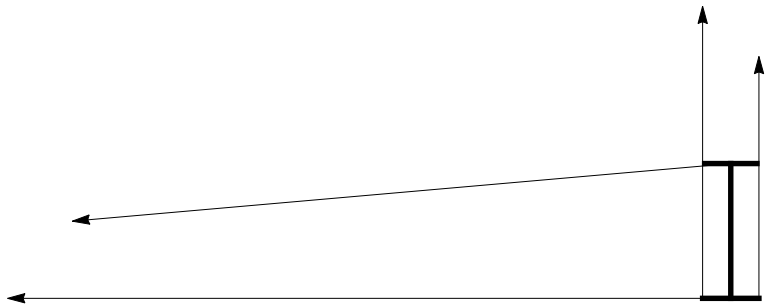

Fig. 7.54 Power-on with locked differential: forces received from the road at $u = 40$ m/s and $\delta = 5°$

7.7 Exercises

7.7.1 Vehicle Kinematic Equations

The vehicle kinematic equations, introduced in Sect. 3.2, are relationships between kinematic quantities. Some of these kinematic quantities (telemetry data) are measured directly on the vehicle. They can then be combined to compute other quantities (mathematical channels). We remind that kinematics is the branch of mechanics concerned with objects in motion, but not with the forces involved.

Playing with real world quantities helps developing quantitative reasoning. Therefore, let us consider the telemetry data measured directly in a race car (Dallara GP2) during one lap of the Barcelona circuit (sample rate is 100 Hz):

- forward velocity u of G (Fig. 7.55);
- vehicle slip angle $\hat{\beta}$ at G (Fig. 7.56);
- yaw rate r (Fig. 7.57);
- longitudinal acceleration a_x of G (Fig. 7.59);
- lateral acceleration a_y of G (Fig. 7.60);
- front wheel steer angle δ_1 (Fig. 7.61).

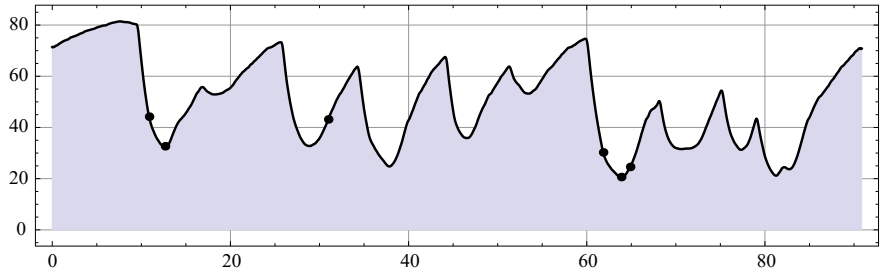

Fig. 7.55 Forward velocity u, in m/s, versus time, in s

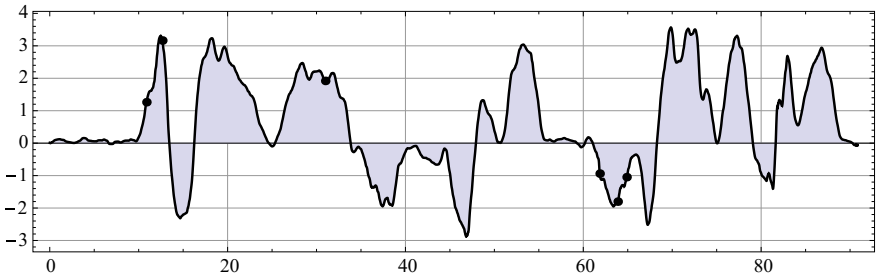

Fig. 7.56 Vehicle slip angle $\hat{\beta}$, in deg, versus time

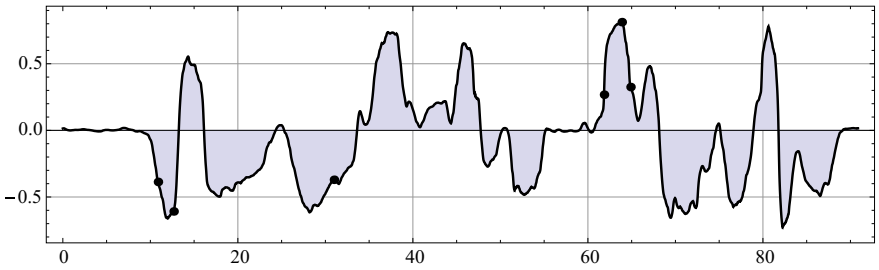

Fig. 7.57 Vehicle yaw rate r, in rad/s, versus time

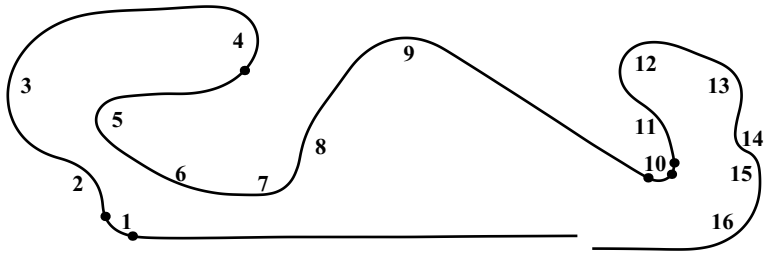

Fig. 7.58 Computed trajectory of the center of mass of a GP2 car. Also shown the six positions of G corresponding to the instants of time of Tables 7.1 and 7.2

All data in Figs. 7.55, 7.56, 7.57, 7.58, 7.59, 7.60 and 7.61 were filtered to reduce noise.

According to (3.16) and (3.18), the lateral velocity $v(t)$ of G is promptly obtained as

$$v(t) = u(t) \tan \hat{\beta}(t) \tag{7.33}$$

As shown in (3.8), the integral of $r(t)$ provides the vehicle yaw angle $\psi(t)$. Then, as discussed in Sect. 3.2.2, the trajectory of G can be obtained. The final result is shown in Fig. 7.58.

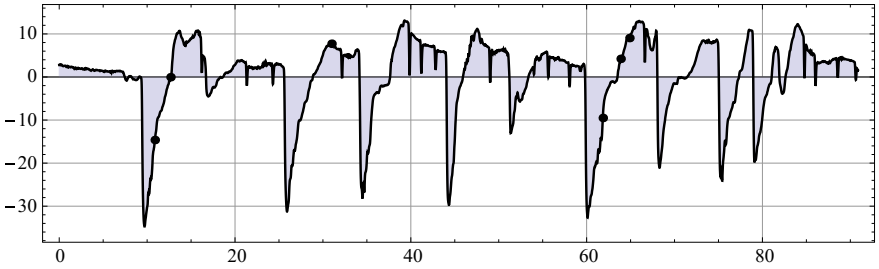

Fig. 7.59 Longitudinal acceleration a_x, in m/s^2, versus time

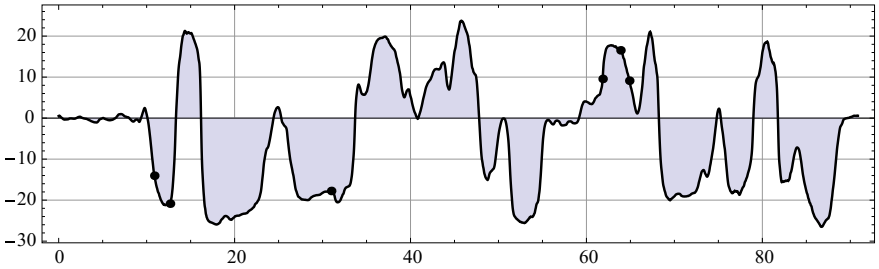

Fig. 7.60 Lateral acceleration a_y, in m/s^2, versus time

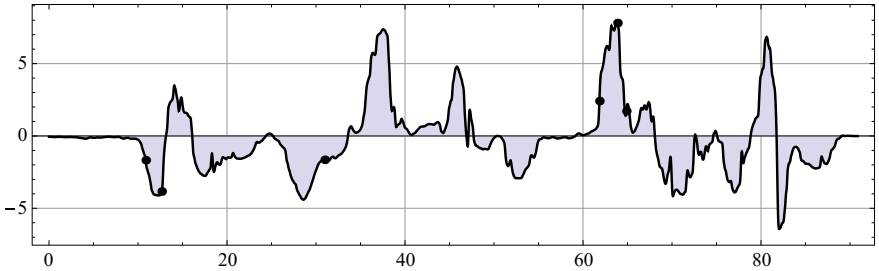

Fig. 7.61 Front wheel steer angle δ_1, in deg, versus time

Typically, the computed trajectory is not a closed curve. This is due to the accumulation of small errors and noise which inevitably affect the measured data. However, in this case the result is pretty good. In Fig. 7.58 all turns of the Barcelona circuit are numbered sequentially, as customary.

The accelerations a_x and a_y are also measured directly, thus avoiding the very unreliable computation of $\dot{u}$ and $\dot{v}$, if we had to employ (3.26) and (3.27).

The plot of the longitudinal acceleration $a_x(t)$ is shown in Fig. 7.59 (negative values mean braking). It is worth noting how sharp are the transitions whenever a braking application begins.

Table 7.1 Samples of measured telemetry data of a GP2 car

	t (s)	turn No	u (m/s)	$\hat{\beta}$ (deg)	r (rad/s)	a_x (m/s^2)	a_y (m/s^2)	δ_1 (deg)
1	10.87	1	44.21	1.26	−0.39	−14.63	−14.05	−1.68
2	12.66	1	32.67	3.16	−0.61	−0.05	−20.86	−3.84
3	30.98	4	43.16	1.92	−0.37	7.72	−17.77	−1.65
4	61.84	10	30.26	−0.94	0.27	−9.52	9.56	2.41
5	63.87	10	20.64	−1.80	0.81	4.22	16.53	7.81
6	64.87	10	24.60	−1.05	0.33	9.05	9.12	1.71

The plot of the lateral acceleration $a_y(t)$ is shown in Fig. 7.60. As expected after (3.27), this plot is similar to that of $r(t)$.

Although not strictly necessary in this framework, also the plot of the front wheel steer angle δ_1 is shown (Fig. 7.61). Quite interestingly, $\hat{\beta}$ and δ_1 always have opposite sign.

As discussed in Sect. 3.2, the measured telemetry data shown in Figs. 7.55, 7.56, 7.57, 7.58, 7.59, 7.60 and 7.61 allow the computation, among others, of the following kinematic quantities as mathematical channels:

- lateral velocity v of G (Eq. (7.33));
- coordinates S and R of the velocity center C in the vehicle frame (Eqs. (3.14) and (3.13));
- radius of curvature R_G of the trajectory of the center of mass G (Eq. (3.36));
- ratios β and ρ (Eqs. (3.16) and (3.17));
- tangential acceleration a_t of G (Eq. (3.34));
- centripetal acceleration a_n of G (Eq. (3.35)).

Values of telemetry data measured at six different instants of time during the same lap are listed in Table 7.1. The corresponding positions of the vehicle on the track are marked by black points in Figs. 7.55, 7.56, 7.57, 7.58, 7.59, 7.60 and 7.61. More precisely, there are two points on turn 1, one point on turn 4 and three points on turn 10. The corresponding values of the mathematical channels listed above are given in Table 7.2. It is strongly recommended to try to figure out what is going on at each of these instants of time.

Values of the angular acceleration $\dot{r}(t)$ are reported in the last column of Table 7.2. As already stated in Sect. 3.2.8, it would be desirable to have sensors to measure directly $\dot{r}$. For the moment we have to compute it as the numerical derivative of the filtered signal $r(t)$. Quite an arbitrary process, as will be shown, e.g., in Fig. 5.23.

After this long introduction, here is the exercise.

Discuss, from a kinematic point of view, the data given in Tables 7.1 and 7.2.

Table 7.2 Computed values (mathematical channels) from the telemetry data of Table 7.1

	t (s)	Turn No	v (m/s)	S (m)	R (m)	R_G (m)	β (deg)	a_t (m/s^2)	a_n (m/s^2)	$\dot{r}$ (rad/s^2)
1	10.87	1	0.96	2.49	−114.30	−142.50	1.25	−14.93	−13.73	−0.32
2	12.66	1	1.80	2.97	−53.70	−51.40	3.16	−1.20	−20.83	0.31
3	30.98	4	1.45	3.90	−116.40	−103.50	1.92	7.12	−18.02	0.02
4	61.84	10	−0.49	1.83	113.10	97.37	−0.93	−9.67	9.41	1.53
5	63.87	10	−0.65	0.80	25.41	25.60	−1.81	3.69	16.65	−0.08
6	64.87	10	−0.45	1.38	75.67	65.21	−1.04	8.88	9.28	−0.52

Solution

Points 1 and 4 have significant negative values of a_x. Moreover, at both points $|a_x| \simeq |a_y|$. Therefore the driver is still braking while entering the turn.

Point 2 is at the so-called apex of the corner, characterized by $|a_x| \simeq 0$ and maximum $|a_y|$.

Points 3, 5 and 6 have positive values of a_x. Therefore, the vehicle is accelerating. It is also exiting the turn, as confirmed by the values of a_y.

In all cases $|\hat{\beta}|$ is very small, and hence $\hat{\beta} \simeq \beta$. Indeed, the lateral velocity v is much lower than u. Nonetheless, (a_x, a_y) are similar, but not almost equal to (a_t, a_n).

The coordinate S of the velocity center C is always positive. Therefore, the vehicle slip angle $\hat{\beta}$ and the front wheel steer angle δ_1 always have opposite sign. The coordinate R of C is usually quite different from the radius of curvature R_G of the trajectory of G. They get closer to each other when the vehicle is near the apex of the corner.

7.7.2 Spin Slip Contributions

According to (3.62), *there are three contributions to spin slip* φ_{ij}. *Discuss their relevance in a GP2 car.*

Solution

From Fig. 7.57, we see that the yaw rate $|r|$ is always lower than 1 rad/s. From Fig. 7.61, we can estimate that the steer angle rate $|\dot{\delta}_{ij}|$ does not exceed 0.5 rad/s, and usually it is much lower. With a camber reduction factor ε_i of about 0.5 and a camber angle γ_{ij} of, say, 4 degrees, the third term ranges between 1 rad/s and 5 rad/s, depending on the value of the wheel angular speed ω_{ij}.

Table 7.3 Coordinates of K and components of $\mathbf{a}_C$, both in the vehicle reference frame, according to the telemetry data of Table 7.1 and to the last column in Table 7.2

	t (s)	Turn No	GK_x (m)	GK_y (m)	$\mathbf{a}_{C_x}$ (m/s^2)	$\mathbf{a}_{C_y}$ (m/s^2)
1	10.87	1	−53.74	20.65	−51.45	2.26
2	12.66	1	27.62	−33.50	15.31	−0.08
3	30.98	4	70.08	−121.20	9.02	−1.70
4	61.84	10	−6.52	−5.91	−182.70	4.26
5	63.87	10	9.23	23.96	5.68	−0.30
6	64.87	10	20.39	−13.35	47.97	0.41

7.7.3 Acceleration Center K and Acceleration of the Velocity Center C

Employing the measured values reported in Table 7.1, along with the values of $\dot{r}$ reported in the last column in Table 7.2, compute in the vehicle reference frame the coordinates of the acceleration center *K and the components of* $\mathbf{a}_C$.

Solution

We can use (3.46) and (3.48). Results are given in Table 7.3. It is worth noting that, in most cases, K and C are quite far apart.

7.7.4 Aerodynamic Downforces

A GP2 race car has the following features (notation as in Sect. 3.7.2):

- $m = 680\,\text{kg}$;
- $a_1/a_2 = 1.27$, that is weight distribution front/rear of 0.44/0.56;
- $S_a\, C_{z1} = 1.5\,\text{m}^2$;
- $S_a\, C_{z2} = 2.1\,\text{m}^2$;
- $S_a\, C_x = 1.1\,\text{m}^2$.

Compute the vertical loads acting on the front axle and on the rear axle when the car is stationary, and when it is running straight at 150 km/h and at 300 km/h.

Solution

The car total weight is $mg = 6670.8\,\text{N}$. Therefore, according to (3.102), the vertical static loads are $Z_1^0 = 0.44 \times 6670.8 = 2935.15\,\text{N}$ for the front axle, and $Z_2^0 = 0.56 \times 6670.8 = 3735.65\,\text{N}$ for the rear axle.

We can now employ (3.80) to evaluate the aerodynamic downforces Z_1^a and Z_2^a when the car has a speed of 150 km/h = 41.67 m/s. The air density is assumed to be $\rho_a = 1.25\,\text{kg/m}^3$. After a simple calculation we get $Z_1^a = 1627.47\,\text{N}$ and $Z_2^a = 2278.46\,\text{N}$.

Therefore, at 150 km/h, according to (3.100), the total vertical load Z_1 acting on the front axle amounts at $Z_1 = Z_1^0 + Z_1^a = 2935.15 + 1627.47 = 4562.62\,\text{N}$, while for the rear axle we obtain $Z_2 = Z_2^0 + Z_2^a = 3735.65 + 2278.46 = 6014.11\,\text{N}$.

The drag force X_a at 150 km/h is equal to 1193.48 N.

Now, let us repeat the computation for a speed of 300 km/h = 83.33m/s. For the aerodynamic downforces on each axle we get $Z_1^a = 6509.90\,\text{N}$ and $Z_2^a = 9113.85\,\text{N}$. Doubling the speed makes the aerodynamic loads four times that much.

At 300 km/h, the total vertical load Z_1 acting on the front axle amounts at $Z_1 = Z_1^0 + Z_1^a = 2935.15 + 6509.90 = 9445.05\,\text{N}$, while for the rear axle we obtain $Z_2 = Z_2^0 + Z_2^a = 3735.65 + 9113.85 = 12849.50\,\text{N}$.

It is interesting to check the front/rear balance of the total loads. It was 0.44/0.56 at zero speed, to become 0.43/0.57 at 150 km/h, and 0.42/0.58 at 300 km/h. Indeed, the front/rear balance of the aerodynamic loads alone is 0.42/0.58.

7.7.5 *Roll Stiffnesses in Formula Cars*

Formula cars, including FSAE cars, have rather flexible tires in the radial direction. The goal of this exercise is to appreciate how much the radial stiffness of the tires can affect the vehicle roll stiffness, and hence the roll motion of the car. This topic is addressed in Sect. 3.10.12. The data are as follows:

- *mass* $m = 305\,\text{kg}$;
- *front track* $t_1 = 1.21\,\text{m}$;
- *rear track* $t_2 = 1.11\,\text{m}$;
- $a_1 = 0.816\,\text{m}$;
- $a_2 = 0.724\,\text{m}$;
- *center of mass height* $h = 0.32\,\text{m}$;
- *front no-roll center height* $q_1 = 0.025\,\text{m}$;
- *rear no-roll center height* $q_2 = 0.045\,\text{m}$;
- *front suspension roll stiffness* $k^s_{\phi_1} = 21740.6\,\text{Nm/rad} = 379.4\,\text{Nm/deg}$;
- *rear suspension roll stiffness* $k^s_{\phi_2} = 22322.2\,\text{Nm/rad} = 389.6\,\text{Nm/deg}$;
- *tire radial stiffness* $p_1 = p_2 = 85000\,\text{N/m}$;
- *grip* $\mu = 1.4$.

Solution

According to (3.121), we compute the front and rear tire roll stiffnesses $k^p_{\phi_1} = 62224.3\,\text{Nm/rad} = 1086.0\,\text{Nm/deg}$ and $k^p_{\phi_2} = 52364.3\,\text{Nm/rad} = 913.9\,\text{Nm/deg}$, respectively.

We see that $k^p_{\phi_1} > k^p_{\phi_2}$ because $t_1 > t_2$. Moreover, as expected, tire roll stiffnesses are bigger than suspension roll stiffnesses, but not that much. More precisely $k^p_{\phi_1}/k^s_{\phi_1} = 2.86$ and $k^p_{\phi_2}/k^s_{\phi_2} = 2.35$.

The roll stiffnesses k_{ϕ_1} and k_{ϕ_2} of the front and rear axles can be computed using (3.119). We obtain with a simple calculation $k_{\phi_1} = 16111.4\,\text{Nm/rad} = 281.2\,\text{Nm/deg}$ and $k_{\phi_2} = 15650.6\,\text{Nm/rad} = 273.2\,\text{Nm/deg}$. Adding these two quantities, as in (3.145), we obtain the vehicle global roll stiffness $k_\phi = 31762.0\,\text{Nm/rad} = 554.4\,\text{Nm/deg}$.

For simplicity, we assume to apply at the center of mass G a lateral force, say, $Y = \mu mg = 4188.9\,\text{N}$. The height $q = 0.036\,\text{m}$ of the no-roll axis under the center of mass is given by (3.137). How much is the vehicle roll angle ϕ?

We are now ready to make a mistake. As a matter of fact, we are tempted to employ the very simple equation (3.154) to estimate the vehicle roll angle ϕ under a lateral force Y. The (wrong) result would be $\phi = 2.15°$.

The correct equation is (3.146), which needs $Y_1 = Ya_2/(a_1 + a_2) = 1968.8\,\text{N}$ and $Y_2 = Ya_1/(a_1 + a_2) = 2220.1\,\text{N}$, and provides the vehicle roll angle $\phi = 2.23°$.

Moreover, by means of (3.143) we can compute the tire roll angles $\phi^p_1 = 0.61°$ and $\phi^p_2 = 0.74°$, and, by means of (3.144) the suspension roll angles $\phi^s_1 = 1.61°$ and $\phi^s_2 = 1.48°$. Of course, they must fulfill (3.130).

With the (wrong) assumption of rigid tires, as in (3.154) with $k_\phi = k^s_{\phi_1} + k^s_{\phi_2} = 44062.8\,\text{Nm/rad} = 769.0\,\text{Nm/deg}$, the (wrong) vehicle roll angle would have been $\phi = 1.55°$.

7.7.6 *Lateral Load Transfers in Formula Cars*

With the data and results of the former exercise, compute the lateral load transfers ΔZ_1 and ΔZ_2.

Solution

Since, as already stated, the tires cannot be assumed as rigid, we have to use (3.138) for computing the lateral load transfers. The results are $\Delta Z_1 = 547.4\,\text{N}$ and $\Delta Z_2 = 610.9\,\text{N}$, which makes $\Delta Z_1/(\Delta Z_1 + \Delta Z_2) = 0.47$.

We know that part of these load transfers come from the suspension links and part from the suspension and tire stiffnesses. Employing (3.150) and (3.151) we obtain $\Delta Z^Y_1 = 40.7\,\text{N}$, $\Delta Z^L_1 = 506.7\,\text{N}$, $\Delta Z^Y_2 = 90.0\,\text{N}$ and $\Delta Z^L_2 = 520.9\,\text{N}$.

Of course, $Yh = \Delta Z_1 t_1 + \Delta Z_2 t_2$.

According to (3.102), the static load on the front axle is $Z^0_1 = 1406.3\,\text{N}$, while on the rear axle it is $Z^0_2 = 1585.8\,\text{N}$. We remind that the static load on each single wheel is not necessarily 50% of the axle load (see p. 103).

For comparison, we repeat the computation assuming (erroneously) rigid tires and get $\Delta Z_1 = 526.5\,\text{N}$ and $\Delta Z_2 = 633.7\,\text{N}$, which makes $\Delta Z_1/(\Delta Z_1 + \Delta Z_2) = 0.45$. This result confirms that tire stiffness has to be taken into account.

We invite the reader to figure out what can be done on the car to end up with the ratio $\Delta Z_1/\Delta Z_2 > 1$, as it should be to have an understeer vehicle.

7.7.7 Centrifugal Force not Applied at the Center of Mass

Going from turn 1 to turn 2 of the Barcelona circuit requires a sharp change in direction, which means fairly high values of $\dot{r}$. *For instance, at the end of turn 1 a Formula car had, at a given instant,* $\dot{r} = 1.56\,\text{rad/s}^2$ *and* $a_y = -8.34\,\text{m/s}^2$. *Assuming* $m = 680\,\text{kg}$ *and* $J_z = 700\,\text{kgm}^2$, *compute how far was the lateral force* Y *from the center of mass* G. *We also know that the steer angle* δ_1 *of the front wheels was only* $0.21°$.

Solution

To answer this question we can rely on (3.98). Indeed, it is precisely x_N the sought for distance. Therefore, we need the lateral force $Y = ma_y = 5671.2\,\text{N}$ and the vertical moment $N = J_z\dot{r} = 1092\,\text{Nm}$. We can assume $N_X \simeq 0$ because the car was going almost straight and hence the limited-slip differential had no effect.

The distance of the lateral (centrifugal) force Y from G is $x_N = N/Y = 0.19\,\text{m}$. As expected, the centrifugal force does *not* act through the center of mass (cf. [11, p. 133]).

7.7.8 Global Aerodynamic Force

Combine the three aerodynamic forces shown in Fig. 7.1 *to obtain the line of action and the magnitude of the global aerodynamic force* F_a.

Solution

We prefer to use a graphic approach. Since forces are applied vectors, we can redraw them only along their line of action. As shown in Fig. 7.62, first we combine X_a and Z_1^a. The resulting vector is then added to Z_2^a, again keeping each force on its line of action, thus obtaining the global aerodynamic force F_a.

It is interesting to compare this result with the analogous result for a road car, shown in Fig. 3.20.

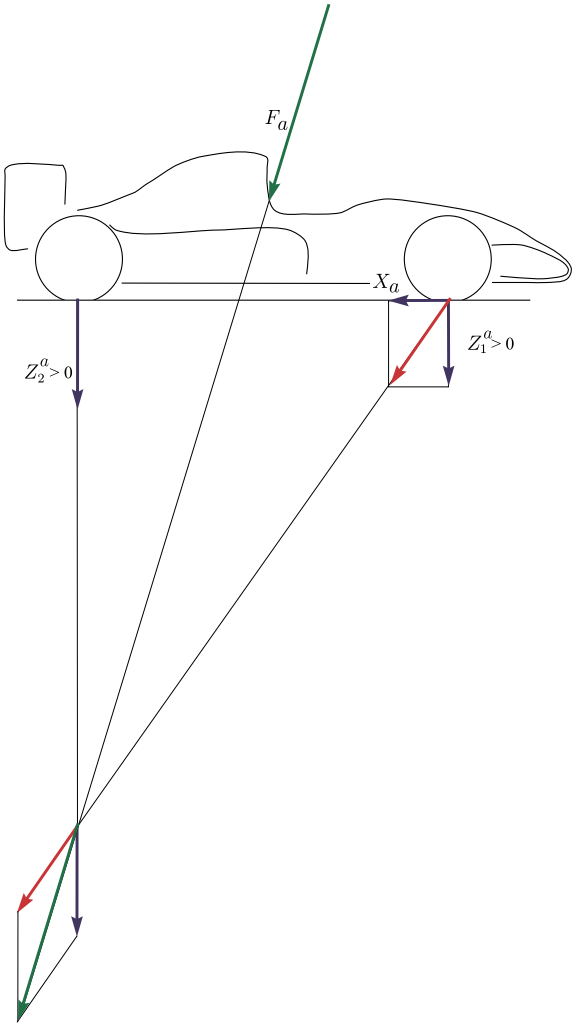

Fig. 7.62 Vectorial sum of the aerodynamic drag and axle downforces to obtain the global aerodynamic force

7.8 Summary

Limited slip differential and wings are typical of race cars. Both greatly impact on the vehicle handling (otherwise they would not be used). Therefore, the first part of this Chapter has been devoted to the formulation of a suitable vehicle model, which, in this case, cannot be single track. As a matter of fact, there is a strong interaction between lateral and longitudinal forces.

The concept of handling diagram becomes inadequate and must be replaced by the handling surface. This fairly new tool has been introduced in the framework of handling of road cars with locked or limited-slip differential.

The handling of Formula cars has been first addressed by means of the handling surface. However, a more powerful description has been provided by means of the *Maps of Achievable Performance - MAP*. With this new approach it is possible to better understand the effects of different vehicle set-ups at steady state and also in power-on/off conditions.

7.9 List of Some Relevant Concepts

p. 339 — Non-open differential makes vehicle behavior very sensitive also to the turning radius. Aerodynamic effects make the vehicle handling behavior very sensitive to the forward speed;
p. 340 — the handling curve must be replaced by the handling surface;
p. 347 — the curves on the handling diagram are the projections of sections of the handling surface;
p. 346 — the yawing moment due to the limited-slip differential can be either positive or negative;
p. 356 — by means of the Map of Achievable Performance (MAP) it is possible to single out the physical grip.

7.10 Key Symbols

a_1	distance of G from the front axle
a_2	distance of G from the rear axle
a_n	centripetal acceleration
a_t	tangential acceleration
a_x	longitudinal acceleration
a_y	lateral acceleration
$\tilde{a}_y$	steady-state lateral acceleration
C	velocity center
C_i	lateral slip stiffness of ith axle
C_x, C_y, C_z	aerodynamic coefficients
d	diameter of the inflection circle
$F_{x_{ij}}$	tire longitudinal force
$F_{y_{ij}}$	tire lateral force
$F_{z_{ij}}$	tire vertical force
g	gravitational acceleration
G	center of mass
h	height of G
J_x, J_y, J_z	moments of inertia
K	acceleration center
K	classical understeer gradient

k_ϕ	total roll stiffness
k_{ϕ_i}	global roll stiffness of ith axle
$k_{\phi_i}^p$	tire roll stiffness
$k_{\phi_i}^s$	suspension roll stiffness
l	wheelbase
m	mass
N	yaw moment
N_β, N_ρ	stability derivatives
N_δ	control derivative
q_1	height of the front no-roll center
Q_1	front no-roll center
q_2	height of the rear no-roll center
Q_2	rear no-roll center
r	yaw rate
R	lateral coordinate of C
r_i	rolling radii
S	longitudinal coordinate of C
S_a	frontal area
t_1	front track
t_2	rear track
u	longitudinal velocity
v	lateral velocity
X	longitudinal force
X_a	aerodynamic drag
Y	lateral force
Y_i	lateral force on the ith axle
Y_β, Y_ρ	stability derivatives
Y_δ	control derivative
Z	vertical force
Z_i	vertical load on ith axle
Z_i^0	static vertical load on ith axle
Z_i^a	aerodynamic vertical load on ith axle
ΔZ	longitudinal load transfer
ΔZ_i	lateral load transfer on ith axle
α_{ij}	tire slip angles
β	ratio v/u
$\hat{\beta}$	vehicle slip angle
β_t	shifted coordinate
(β_y, β_δ)	gradient components
γ_{ij}	camber angles
δ_{ij}	steer angle of the wheels
δ_v	steering wheel angle of rotation
ε_1	Ackermann coefficient

ζ	exponent
ζ	damping ratio
η_h	internal efficiency of the differential housing
ρ	ratio r/u
ρ_a	air density
ρ_t	shifted coordinate
(ρ_y, ρ_δ)	gradient components
$\sigma_{x_{ij}}$	tire longitudinal slips
$\sigma_{y_{ij}}$	tire lateral slips
τ	steer gear ratio
ϕ	roll angle
Φ_i	slope of the axle characteristics
φ_{ij}	spin slips
ψ	yaw angle
ω_h	angular velocity of the differential housing
ω_{ij}	angular velocity of the rims
ω_n	natural angular frequency
ω_s	damped natural angular frequency

References

1. Bastow D, Howard G, Whitehead JP (2004) Car suspension and handling, 4th edn. SAE International, Warrendale
2. Dixon JC (1991) Tyres, suspension and handling. Cambridge University Press, Cambridge
3. Font Mezquita J, Dols Ruiz JF (2006) La Dinámica del Automóvil. Editorial de la UPV, Valencia
4. Frendo F, Greco G, Guiggiani M (2006) Critical review of handling diagram and understeer gradient for vehicles with locked differential. Vehicle Syst Dyn 44:431–447
5. Frendo F, Greco G, Guiggiani M, Sponziello A (2007) The handling surface: a new perspective in vehicle dynamics. Vehicle Syst Dyn 45:1001–1016
6. Frendo F, Greco G, Guiggiani M, Sponziello A (2008) Evaluation of the vehicle handling performances by a new approach. Vehicle Syst Dyn 46:857–868
7. Gillespie TD (1992) Fundamentals of vehicle dynamics. SAE International, Warrendale
8. Pacejka HB (1973) Simplified analysis of steady-state turning behaviour of motor vehicles, part 1. Handling diagrams of simple systems. Vehicle Syst Dyn 2:161–172
9. Pacejka HB (1973) Simplified analysis of steady-state turning behaviour of motor vehicles, part 2: Stability of the steady-state turn. Vehicle Syst Dyn 2:173–183
10. Pacejka HB (1973) Simplified analysis of steady-state turning behaviour of motor vehicles, part 3: More elaborate systems. Vehicle Syst Dyn 2:185–204
11. Seward D (2014) Race car design. Palgrave, London
12. Wong JY (2001) Theory of ground vehicles. Wiley, New York